TECHNICAL REPORT S-71-15

DEVELOPMENT OF A DYNAMIC HIGH-PRESSURE TRIAXIAL TEST DEVICE

by

J. Q. Ehrgott, R. C. Sloan

November 1971

Sponsored by Defense Nuclear Agency

Conducted by U. S. Army Engineer Waterways Experiment Station, Vicksburg, Mississippi

TECHNICAL REPORT S-71-15

DEVELOPMENT OF A DYNAMIC HIGH-PRESSURE TRIAXIAL TEST DEVICE

by

J. Q. Ehrgott, R. C. Sloan

November 1971

Sponsored by Defense Nuclear Agency
DNA Subtask SB209A

Conducted by U. S. Army Engineer Waterways Experiment Station, Vicksburg, Mississippi

ARMY-MRC VICKSBURG, MISS

ABSTRACT

A unique dynamic high-pressure triaxial test device has recently been developed at the U. S. Army Engineer Waterways Experiment Station to assist in obtaining dynamic stress-strain and strength data for use in formulating soil and rock constitutive relations used in blast-induced ground shock calculations. The device is capable of imposing controlled impulsive-type confining pressures up to 15 kips/in^2 on specimens up to 3 inches in diameter; peak pressures can be achieved in as little time as 3 msec, and all pressure can be removed in 20 msec. These dynamic confining pressures can be time-synchronized with similar dynamic axial load pulses with magnitudes up to 100 kips. Independent control of the axial and radial stresses permits application of dynamic hydrostatic loadings and unloadings to obtain bulk moduli; dynamic deviatoric loadings under constant confining pressure to obtain Young's moduli and yield stress data; dynamic deviatoric loadings while maintaining a condition of constant mean normal stress to obtain shear moduli; and a variety of other loadings including constant stress ratios.

This report presents a description of the dynamic high-pressure triaxial device, which consists basically of five components, i.e., the rise pressure supply system, the decay system, the base assembly, the triaxial chamber, and the stroke limiter. Details of the measurement systems used for determination of confining pressure, axial load, and axial and lateral deformation under dynamic high-pressure fluid environments are given.

Several results from an evaluation test series conducted on field NX-size cores of a clayey siltstone and Cretaceous sandstone are presented to demonstrate some of the capabilities of the device and to show the type of dynamic stress paths the device is capable of generating. The data are shown as time-history plots of confining pressure and axial load for the complete hydrostatic and shear phases of the tests along with the corresponding stress path plots of deviator stress versus mean normal stress. Deviator stress versus axial strain plots are also shown for the shear phase.

The results illustrate that the device is not only useful in site

investigations in which determination of dynamic properties of the material encountered is required for engineering design purposes, but also in fundamental research studies to determine material behavior under a variety of states of impulsive-type stresses.

PREFACE

The dynamic high-pressure triaxial test device, support equipment, and laboratory procedures described herein were developed in conjunction with one part of the continuing research on "Propagation of Ground Shock Through Earth Media" sponsored by the Defense Nuclear Agency (DNA) under DNA Subtask SB209A. This study was conducted during the period July 1968 through July 1970 by personnel of the Soils Division, U. S. Army Engineer Waterways Experiment Station (WES).

The main text of this report was prepared by Mr. J. Q. Ehrgott, Impulse Loads Section (ILS), Soil Dynamics Branch, Soils Division, WES, under the direct supervision of Mr. J. G. Jackson, Jr., Chief, ILS. Appendix A was prepared by Mr. R. C. Sloan, ILS, who also provided helpful guidance in the preparation of the main text. Mr. R. W. Cunny was Chief of the Soil Dynamics Branch, and Mr. J. P. Sale and Mr. R. G. Ahlvin were Chief and Assistant Chief, respectively, of the Soils Division.

Directors of the WES during the conduct of the study and preparation of this report were COL Levi A. Brown, CE, and COL Ernest D. Peixotto, CE. Technical Directors were Mr. J. B. Tiffany and Mr. F. R. Brown.

CONTENTS

ABSTRACT---- 4

PREFACE---- 6

CONVERSION FACTORS, BRITISH TO METRIC UNITS OF MEASUREMENT---- 9

CHAPTER 1 INTRODUCTION---- 10

CHAPTER 2 DESCRIPTION OF THE DYNAMIC HIGH-PRESSURE TRIAXIAL TEST EQUIPMENT---- 11

2.1 Pressure Supply System---- 12
2.2 Base Assembly---- 13
2.3 Pressure Decay System---- 14
2.4 Triaxial Chamber---- 15
2.5 Stroke Limiter---- 15
2.6 Operating Controls---- 16

CHAPTER 3 MEASUREMENT SYSTEM---- 25

3.1 Pressure Measurement---- 25
3.2 Load Measurement---- 26
3.3 Specimen Deformation Measurement---- 27
3.4 Recording System---- 28
3.5 Specimen Placement Procedure---- 28

CHAPTER 4 PERFORMANCE TESTS---- 37

4.1 First Test Series---- 37
4.2 Second Test Series---- 40
4.3 Third Test Series---- 44
4.4 Future Investigations---- 47

CHAPTER 5 CONCLUSION AND FUTURE PLANS---- 60

5.1 Conclusion---- 60
5.2 Future Plans---- 60

APPENDIX A 100-KIP DYNAMIC RAM LOADER---- 61

A.1 Design Considerations---- 61
A.2 Operation of Loader---- 62
A.3 Dynamic Load Application---- 62
A.4 Static Load Application---- 64

REFERENCES---- 67

FIGURES

2.1 DHT device in assembled test position---- 18
2.2 Schematics of the pressure supply system showing various stages of its operation---- 19
2.3 Plan view and cross section of the multimetering orifice---- 20
2.4 Cross section of the base assembly---- 21

2.5 Cross sections of the base assembly and decay system illustrating various stages during pressure decay---------- 22
2.6 Cross section of the triaxial chamber---------- 23
2.7 Cross section of the stroke limiter---------- 24
3.1 WES pressure transducer and wiring schematic---------- 30
3.2 High-capacity piston load cell and wiring schematic---------- 31
3.3 Low-capacity base load cell and wiring schematic---------- 32
3.4 Vertical deformeter and wiring schematic---------- 33
3.5 Lateral deformeter and wiring schematic---------- 34
3.6 Schematic of the electrical circuit for the recording system---------- 35
3.7 Special instrumentation package with a rock specimen in place---------- 36
4.1 Representative pressure versus time plot showing pulse characteristics of very fast rise times---------- 48
4.2 Representative pressure versus time plot showing pulse characteristics of moderate rise times---------- 48
4.3 Desired time-history plots of pressure and load used in the determination of control settings---------- 49
4.4 Time-history plots of pressure and load based on measured data---------- 50
4.5 Results of Test 2.1 on clayey siltstone showing the measured time-history plot of pressure and load and the calculated stress path---------- 51
4.6 Results of Test 2.2 on clayey siltstone showing the measured time-history plot of pressure and load and the calculated stress path---------- 52
4.7 Results of Test 2.3 on clayey siltstone showing the measured time-history plot of pressure and load and the calculated stress path---------- 53
4.8 Results of Test 2.4 on clayey siltstone showing the measured time-history plot of pressure and load and the calculated stress path---------- 54
4.9 Combined plot of deviator stress versus axial strain during the shear phase of the tests of four clayey siltstones------- 55
4.10 Results of Test 3.1 on sandstone showing measured data and calculated stress path and stress-strain plot---------- 56
4.11 Results of Test 3.2 on sandstone showing measured data and calculated stress path and stress-strain plots---------- 57
4.12 Results of Test 3.3 on sandstone showing measured data and calculated stress path and stress-strain plots---------- 58
4.13 Results of Test 3.4 on sandstone showing measured data and calculated stress path and stress-strain plots---------- 59
A.1 The 100-kip dynamic ram loader with the dynamic high-pressure triaxial device in the assembled test position------ 65
A.2 Actuator of the 100-kip dynamic loader---------- 66

CONVERSION FACTORS, BRITISH TO METRIC UNITS OF MEASUREMENT

British units of measurement used in this report can be converted to metric units as follows.

Multiply	By	To Obtain
inches	2.54	centimeters
feet	0.3048	meters
square inches	6.4516	square centimeters
pounds	0.45359237	kilograms
pounds per square inch	0.070307	kilograms per square centimeter
kips	453.59237	kilograms
kips per square inch	70.307	kilograms per square centimeter
inches per second	2.54	centimeters per second

CHAPTER 1

INTRODUCTION

The U. S. Army Engineer Waterways Experiment Station (WES), under sponsorship of the Defense Nuclear Agency, has recently developed a unique dynamic high-pressure triaxial testing device (DHT). The device permits acquisition of both axial and lateral deformation data while undisturbed soil and/or rock specimens are subjected to various states of controlled impulsive-type stresses produced by varying both the axial stress and the radial stress rapidly with time. The device is used to develop controlled dynamic pressure pulses within the triaxial chamber fluid on soil or rock test specimens up to 3 inches[1] in diameter. Controlled dynamic axial pulse loads are delivered to the specimen by a piston that is driven by an existing pneumatic ram loader (SECO, as described in Appendix A). The DHT consists of a triaxial cell and a pressure supply and decay system that permits the chamber pressure to be varied with time. Together the DHT and SECO operate in a testing program in such a manner as to apply time-varying confining pressures and axial loads to test specimens at independently controlled (but synchronized), programmed rise, hold, and decay times. Rise time is defined as the time from zero load or pressure to peak load or pressure, hold time is the time of constant peak load or pressure, and decay time is the time from peak load or pressure to zero load or pressure. The maximum dynamic confining pressure attainable is approximately 15,000 psi, and the fastest rise and decay times are 3 and 20 msec, respectively.

This report presents a description of the DHT, the necessary support equipment, and details of the measurement system. Results of performance evaluation tests conducted on clayey siltstone and a Cretaceous sandstone are presented since they demonstrate some of the capabilities of the device and show some of its characteristics.

---

[1] A table of factors for converting British units of measurement to metric units is presented on page 9.

CHAPTER 2

DESCRIPTION OF THE DYNAMIC HIGH-PRESSURE TRIAXIAL TEST EQUIPMENT

Development of a high-pressure, dynamic, laboratory testing device was required to study the behavior of earth material subjected to a variety of states of dynamic stress. Selection of a triaxial test for this purpose was made based on the known versatility of the test and the great amount of information and data available from conventional triaxial tests conducted over the years. Although other suitable test configurations of different boundary conditions could have been developed, it is believed that much more time and money would have had to be spent in analyzing and interpreting test results, correlating material properties obtained from other tests, and gaining engineering experience on the actual application of test results to design problems. The selection of both the pressure level (15,000 psi) and dynamic rate (rise time of 3 msec) was based on need for complete material property information within the range required for immediate application to existing engineering and research problems in the area of nuclear weapons effects and for operational compatibility with the existing support equipment such as the SECO dynamic loader. Since fast-opening, large-flow valves had already been developed for ram-type loaders, the employment of a similar pneumatic pressure system to produce the fluid chamber pressure was considered the most feasible approach. The measurement system is similar to that previously developed and used at WES on conventional high-pressure triaxial test equipment.

The DHT was designed and fabricated as a joint effort between WES and SECO-DYN, Inc. It employs a conventional triaxial test chamber configuration common to soil and rock mechanics and consists of five separate components: the pressure supply system, the pressure decay system, the base, the chamber, and the stroke limiter. The fluid chamber pressure impulse characteristics are controlled by the combined action of the pressure rise and pressure decay systems. The chamber pressure is developed by the force of compressed nitrogen acting on an amplifying piston in the base. The stroke limiter provides control of the axial loading piston's maximum

travel. The assembled components are attached to a main base plate, which in turn rests on a skid plate that provides for placement of the device under the SECO dynamic loader. Figure 2.1 shows the device in test position under the SECO dynamic loader.

2.1 PRESSURE SUPPLY SYSTEM

The chamber fluid pressure is developed by relatively low-pressure compressed gas from the pressure supply system acting on a differential-area amplifying piston located in the base. The pressure supply system stores the compressed gas, and upon an electrically controlled signal, a fast-opening valve releases the gas. The gas then flows through a multimetering orifice to the base and acts on the amplifier piston at a controlled rate. This moves the amplifier piston up into the chamber and creates the confining pressure in the fluid surrounding the test specimen. The level of gas pressure stored in the two large reservoir tanks prior to a test is determined by computing the gas pressure required to act on the large-area bottom side of the amplifier piston to produce the desired chamber pressure developed on the smaller area top side of the amplifier piston. A large-diameter fast-opening valve in a closed position contains the gas in the reservoirs. The valve is actuated on an electrically controlled signal by a separate operating system using compressed gas to power the valve. Opening time of the valve is less than 1 msec. Once the valve is opened, the compressed gas enters the main flow orifice and passes through a multimetering orifice that controls the rate of flow to the base. Manual adjustment of the multimetering orifice determines the pressure rise time; the larger the opening, the faster the rise time. Rise times from 3 to 1,000 msec may be obtained.

Figure 2.2a shows a schematic of the pressure supply system with the fast-opening valve in the closed position as it would be prior to a test. A gas pressure of 750 psi in chamber RC is used to close the valve, thus blocking the two reservoir ports, and a valve-open pressure of 500 psi is introduced in chamber RC, as shown in Figure 2.2a. The valve is locked in the closed position by allowing gas pressure of 750 psi to act on the fluid in chamber O, as shown in Figure 2.2b. The areas over which the water

pressure acts are such that the valve remains closed even against the valve-open pressure in chamber RO. The gas pressure in chamber RC is then exhausted. In this condition, as shown in Figure 2.2c, the valve is ready for activation. Since water is relatively incompressible (as compared with gas), release of only a small amount of the water reduces the water pressure to zero almost instantaneously. The 750-psi pressure in chamber RO is unbalanced, as shown in Figure 2.2d, and causes the valve to open very rapidly. A valve decelerator prevents equipment damage by providing for a gradual arresting of the valve's motion. The final open position of the valve is shown in Figure 2.2e.

The multimetering orifice consists of two large plugs, each the diameter of the main flow orifice and each containing a small-diameter orifice for small flow adjustments. The large plugs permit the orifice area to be varied over a range sufficient to provide for flow rate times of from approximately 150 to 3 msec. When the two plugs are closed, the small plugs contained within the larger plugs may be used and the orifice area can be adjusted to obtain flow rate times of up to 1,000 msec. A schematic of the multimetering orifice is shown in Figure 2.3. Prior calibrations of rise time versus flow area permit adjustment of the multimetering orifice to produce the desired test results.

2.2 BASE ASSEMBLY

A schematic of the base assembly is shown in Figure 2.4. The outside dimensions are 13-1/2 by 13-1/2 inches. The assembly contains a large center bore approximately 11 inches in diameter. The pressure supply system is connected to one side of the base by a 4-inch-diameter port. The gas from the pressure supply system flows through the port and is channeled around the inner periphery of the base to produce an even pressure on the lower surface of the amplifier piston. On the side opposite the pressure supply entry port are two 1-1/2-inch-diameter ports connecting the pressure decay system to the base. A 3-1/2-inch-diameter base pedestal extends through the amplifier piston into the triaxial chamber and provides a support for the specimens and instrumentation units. The triaxial chamber is attached to the base by means of large ACME threads.

The amplifier piston, contained in the base, uses realtively low gas pressure from the pressure supply system to generate a much higher fluid pressure in the triaxial chamber. The lower surface area of the piston on which the gas acts is 75.4 in^2, and the top surface area, which extends into the fluid-filled triaxial chamber, is 10.0 in^2. This provides for an area ratio of 7.54. For every 1 psi of gas acting on the lower surface, the piston will move upward, increasing the fluid chamber pressure approximately 7.54 psi. The chamber, when filled with fluid (hydraulic oil), requires an upward travel of approximately 1.8 inches of the amplifying piston to produce a pressure of 15,000 psi during the dynamic test. Other factors, such as "O" ring friction and the inertia resulting from rapid acceleration and deceleration of the piston in a dynamic test, will tend to cause variations in the actual fluid pressure, which will be discussed later. Rubber impact pads attached to the upper and lower surfaces of the piston prevent metal-to-metal slapping in the dynamic tests.

2.3 PRESSURE DECAY SYSTEM

The pressure decay system is connected to the base on the side opposite the rise pressure supply system. This system consists of a 1-1/2-inch-diameter fast-opening valve and multimetering orifice. The purpose of the decay system is to provide controlled pressure decay of the triaxial chamber fluid with programmable decay times from 20 to 10,000 msec. This is accomplished by channeling the gas at a controlled rate from under the amplifying piston to the top side as illustrated in Figure 2.5. Figure 2.5a shows the base and decay system with the compressed gas from the pressure supply system acting on the underside of the amplifying piston causing pressure to be developed in triaxial chamber fluid. Figure 2.5b illustrates the initiation of the pressure decay phase, with the decay valve open and gas just starting to flow through the multimetering orifice. Figure 2.5c shows the gas acting on both sides of the amplifying piston, causing equalization of gas pressure across the piston, thereby allowing the fluid pressure to dissipate by pushing the piston down to its original position.

2.4 TRIAXIAL CHAMBER

The triaxial chamber is connected to the base by large ACME threads that provide for easier assembly and protection against cross threading. Extending up into the chamber is a 3-1/2-inch-diameter base pedestal and a 3-1/2-inch-ID by 5.0-inch-OD amplifying piston. A stroke limiter containing the axial loading piston extends into the chamber from the top and will be discussed in the next section. The internal dimensions of the chamber are 5.0 inches in diameter by approximately 11.0 inches in height. Figure 2.6 shows a cross section of the chamber containing a special steel specimen used for calibration purposes.

2.5 STROKE LIMITER

Figure 2.7 shows a cross section of the stroke limiter attached to the top of the triaxial chamber. Since the ram of the SECO dynamic loader may travel 5 inches during load application, the stroke limiter is required in order to provide limiting control of travel from 0 to 2 inches of the axial load piston. This prevents damage to the test device after specimen failure. The stroke limiter also prevents damage to the test device when the confining chamber pressure is still acting while the axial load is being decayed quickly by arresting the resulting upward motion of the axial loading piston. The stroke limiter also allows height adjustments of the initial position of the axial piston. The adjustments are required because of slight differences in the length of each specimen.

The downward motion of both the SECO ram and the axial piston is arrested after a specimen failure by contact of the loading plate with the impact pad on the top surface of the adjustment plug. The upward travel of the axial piston is arrested by the limiter piston plug contacting the impact pad on the bottom surface of the adjustment plug. The adjustment plug provides for height adjustments of the axial loading piston to accommodate various lengths of test specimens. The limiter piston plug provides for adjustment of stroke travel from approximately 0 to 2 inches. Both adjustments are made prior to each test. It should be pointed out that since only materials that have relatively small strains at failure would require

the higher levels of load, it was not necessary to design a system capable of taking the energy produced by 100 kips traveling over the full 2 inches. Reduction of the stroke travel is required for high load levels.

2.6 OPERATING CONTROLS

Manual and electrical controls are required in the operation of the DHT. The manual controls, which have been mentioned in the discussion of the various system components, are set prior to each test. The chamber pressure, rise time, decay time, and axial piston's stroke are all set by manually operated controls. An electrical control system is actually used to control the initiation of valve openings, which, along with the multimetering orifice settings, control the pulse time characteristics of the confining pressure and axial load during the test. Programmable electrical counters are used to activate the fast-opening rise valves and the fast-opening decay valves at preselected time intervals. The electrical controls of the DHT are separated from, but capable of being synchronized with, the electrical control system of the SECO ram loader, thereby permitting application of a nearly infinite variety of combinations of chamber pressures and axial load pulses to the test specimen. The control system also activates an oscillograph used to record test data from the various measurement units.

The following procedure is given to illustrate how a test is conducted when only a dynamic confining pressure is to be applied to a specimen. The desired pulse characteristics are as follows: a rise time of 5 msec, a hold time of 10 msec, and a decay time of 30 msec. The multimetering orifice on the rise system is adjusted to allow a complete gas flow in 5 msec based on the calibration curve of rise time versus flow area. For this case, it requires that the large plug be almost completely opened. Likewise, the decay system's multimetering orifice is adjusted for a 30-msec decay. The electrical timers are set in the following order with the reference time of 0000 msec controlled by the test initiate switch.

1. To initiate rise valve, control 1 is set at 0500 msec. The initial 500 msec to the opening of the rise valve gives the oscillograph time to build up the proper recording paper speed of 160 in/sec.

2. To initiate decay valve, control 2 is set at 0515 msec. The time to the opening of the decay valve of 15 msec includes the 5-msec rise time and the 10-msec hold time during which the fluid pressure within the chamber is maintained at peak pressure.

3. To stop the oscillograph, control 3 is set at 0600 msec. The time to full decay is actually 35 msec; therefore, the timer could have been set at 0550 msec. However, experience has shown that allowing some additional time for oscillograph cutoff beyond actual test completion insures a constant recorder paper speed throughout the test.

The DHT is assembled and bolted down, and both the rise valve and the decay valve are closed and their individual systems set up ready to activate. The reservoir tanks are filled to the gas pressure necessary to effect the desired fluid pressure. The operator then initiates the test by a switch that activates all the electrical timer controls. At the end of the test, the operator then manually exhausts the gas still contained within the system.

For tests requiring the DHT and the SECO, two additional electrical timers are employed to operate the SECO rise valve and decay valve. Again, time is referenced from the closing of the test initiate switch. A separate control console is also used to set up the SECO, but test initiation is accomplished by the same switch as mentioned above.

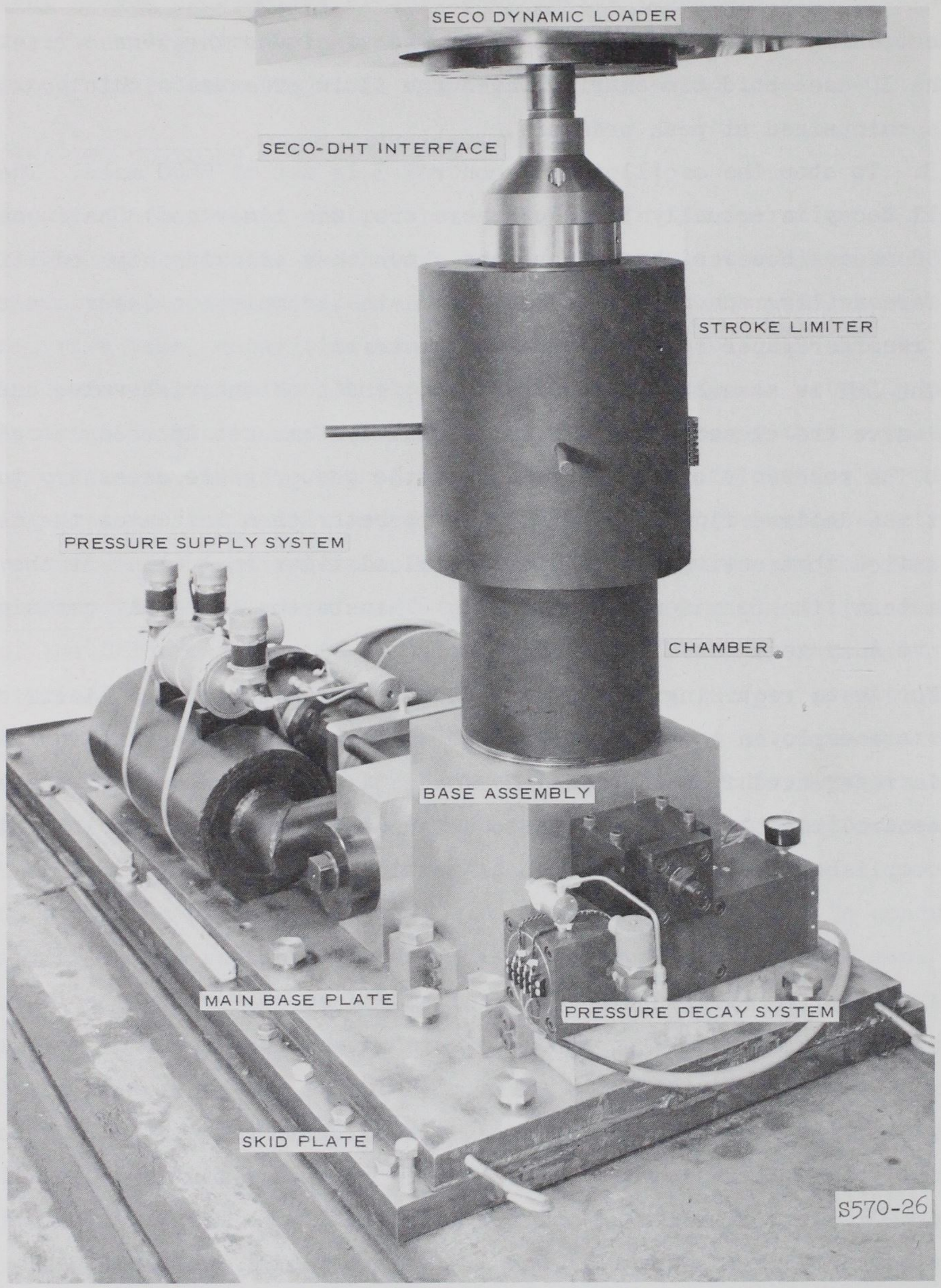

Figure 2.1 DHT device in assembled test position.

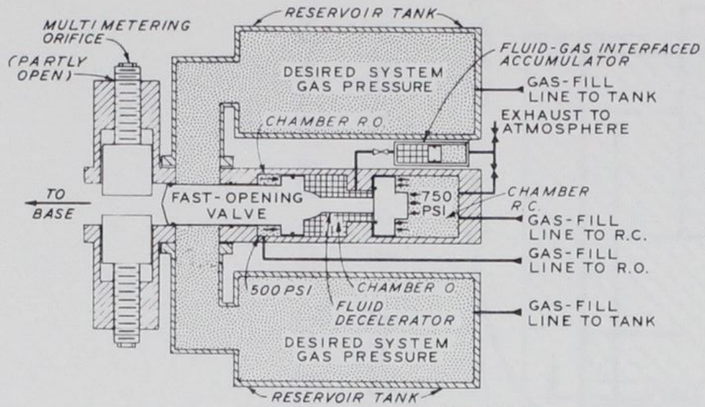

a. RISE PRESSURE SUPPLY SYSTEM FOLLOWING VALVE CLOSURE AND APPLICATION OF SYSTEM GAS PRESSURE

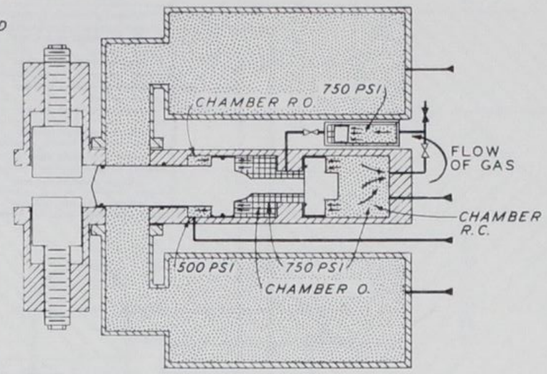

b. PRESSURIZATION OF CHAMBER O

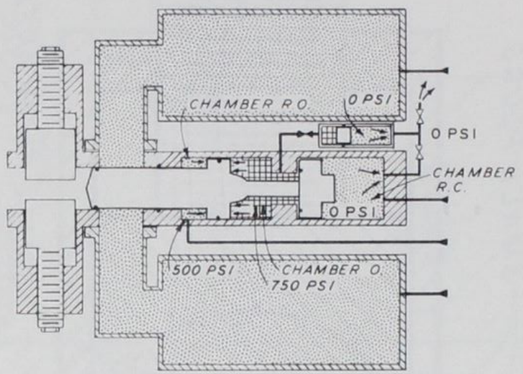

c. RELEASE OF THE PRESSURE IN CHAMBER R.C

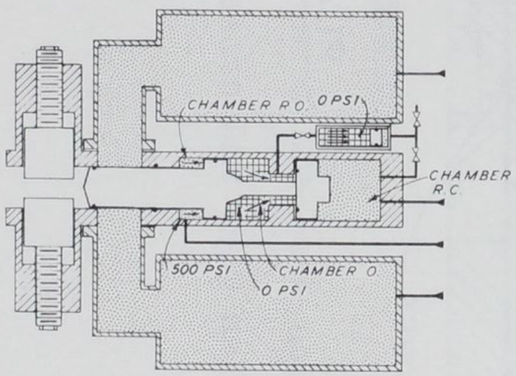

d. ACTUAL INITIATION OF VALVE OPENING DUE TO RELEASE OF WATER PRESSURE IN CHAMBER O

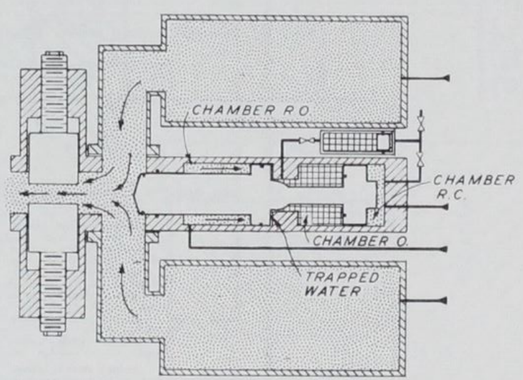

e. AFTER OPENING OF THE FAST-OPENING VALVE SHOWING FLOW OF SYSTEM GAS PRESSURE TO THE BASE

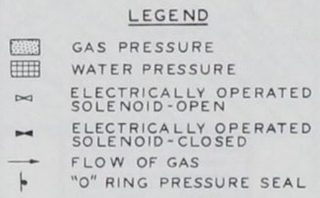

Figure 2.2 Schematics of the pressure supply system showing various stages of its operation.

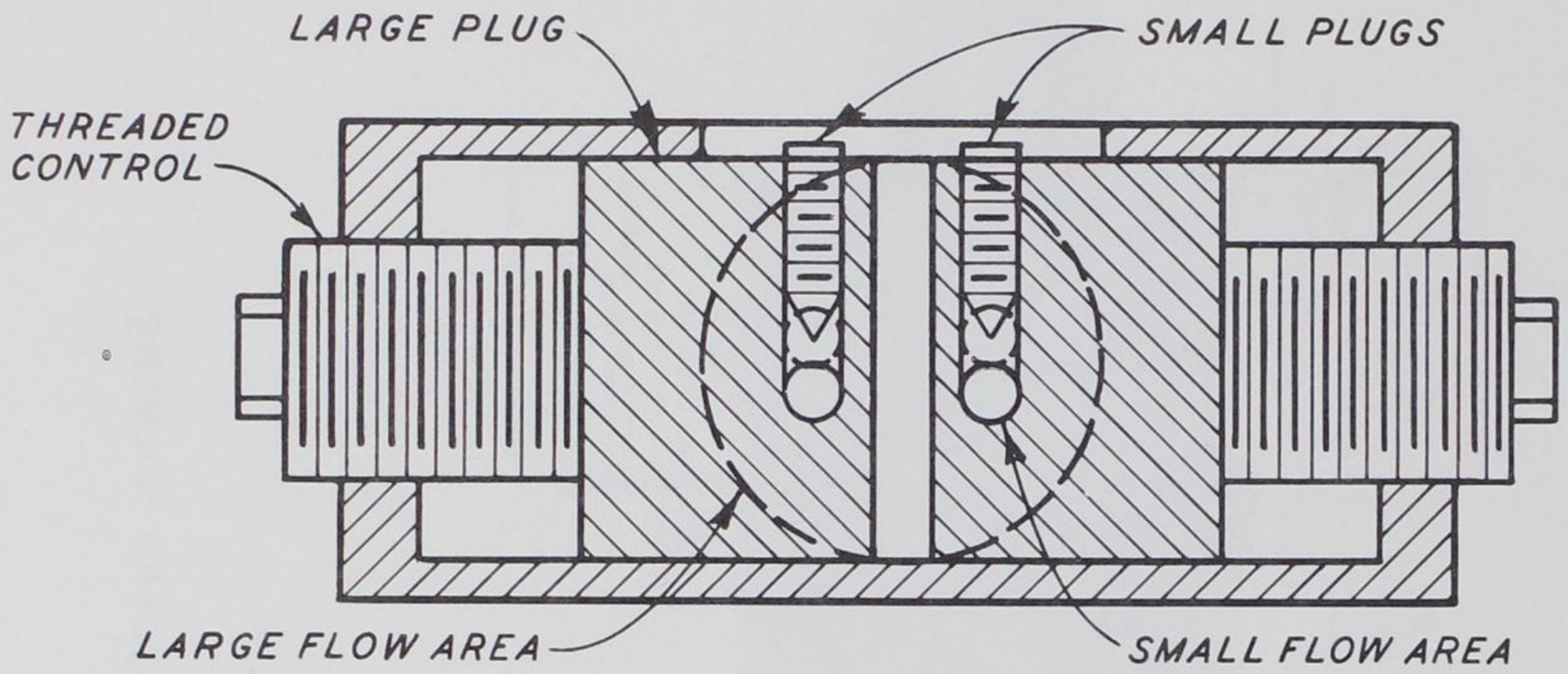

SECTION

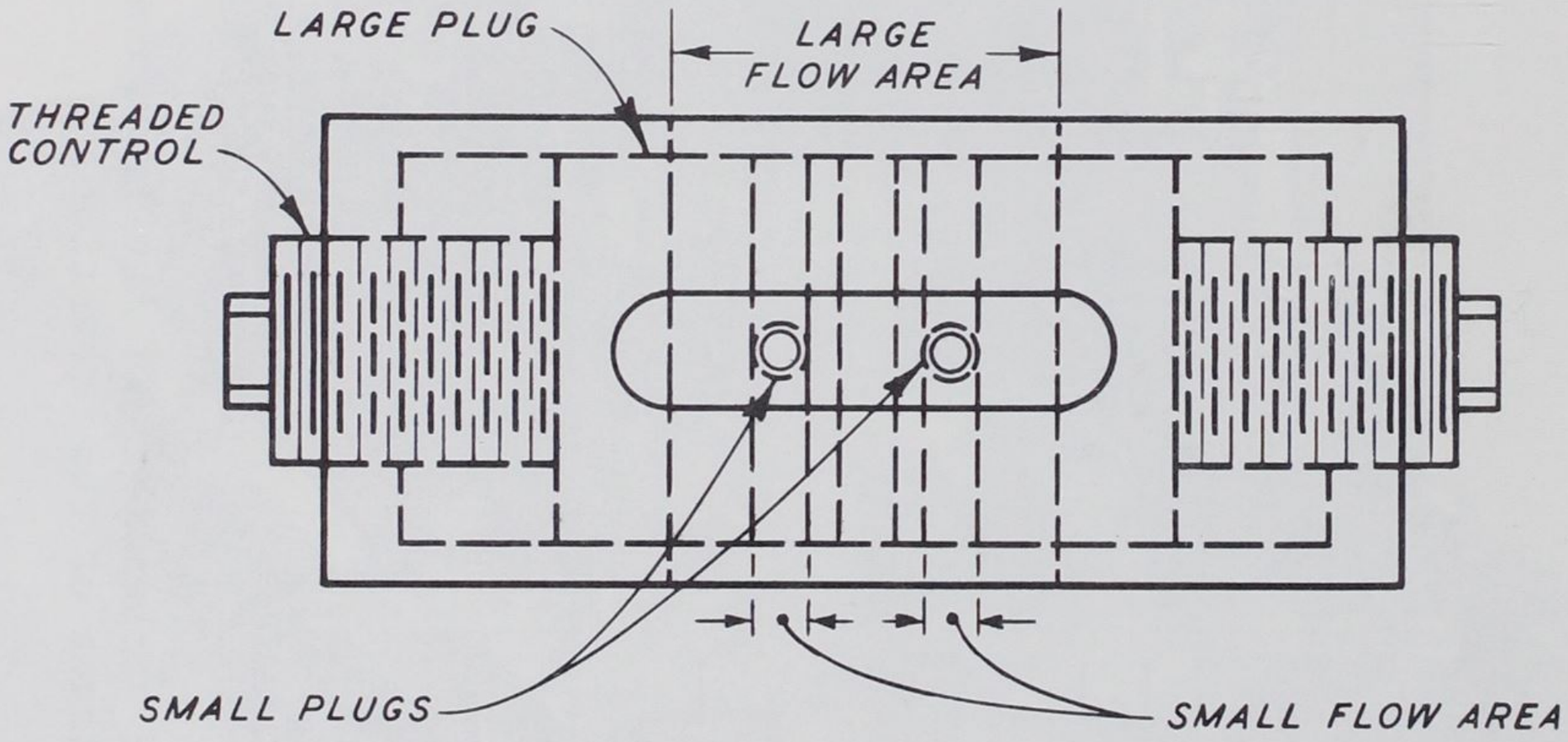

PLAN

Figure 2.3 Plan view and cross section of the multimetering orifice.

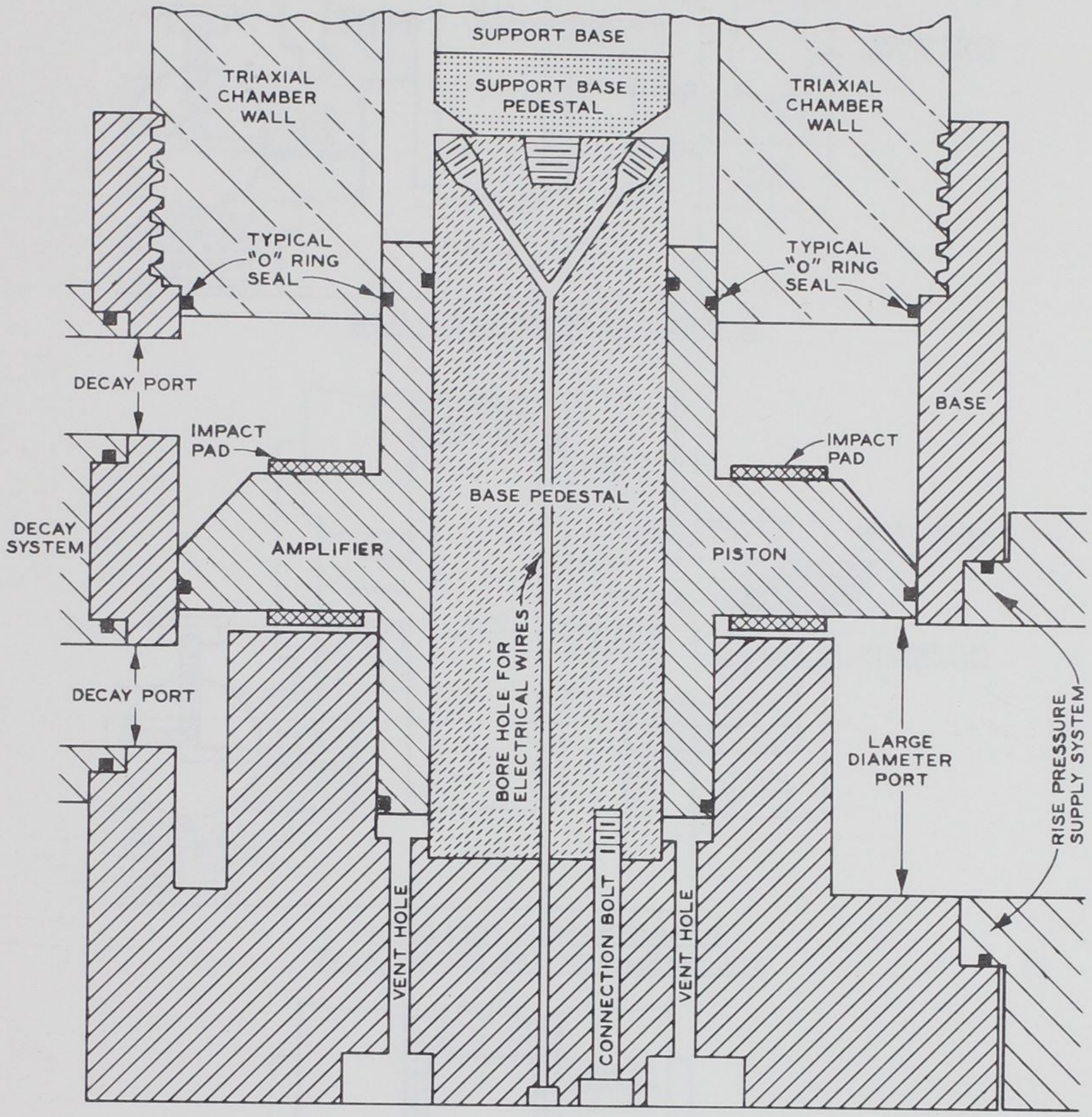

CROSS SECTION

Figure 2.4 Cross section of the base assembly.

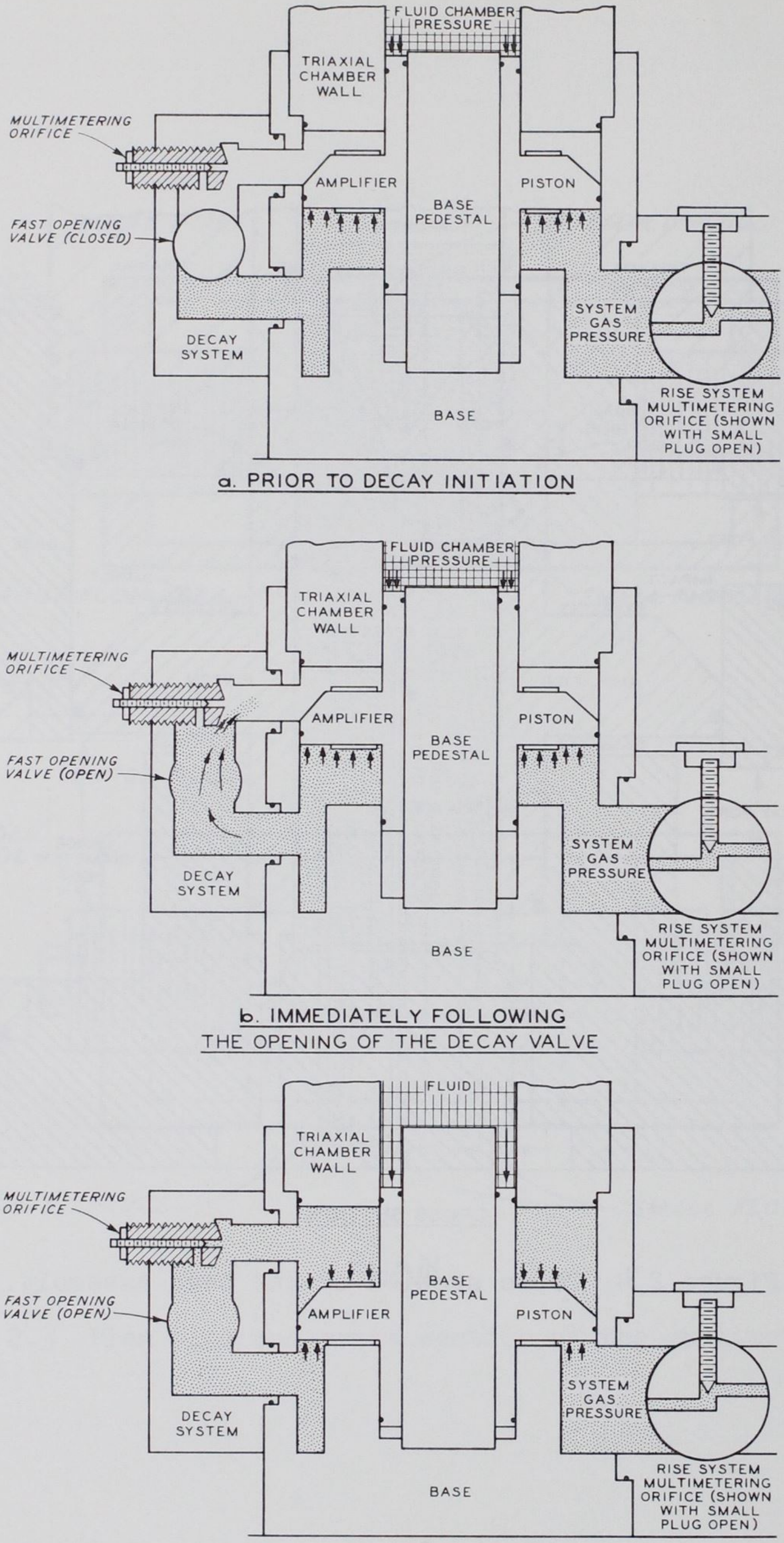

Figure 2.5 Cross sections of the base assembly and decay system illustrating various stages during pressure decay.

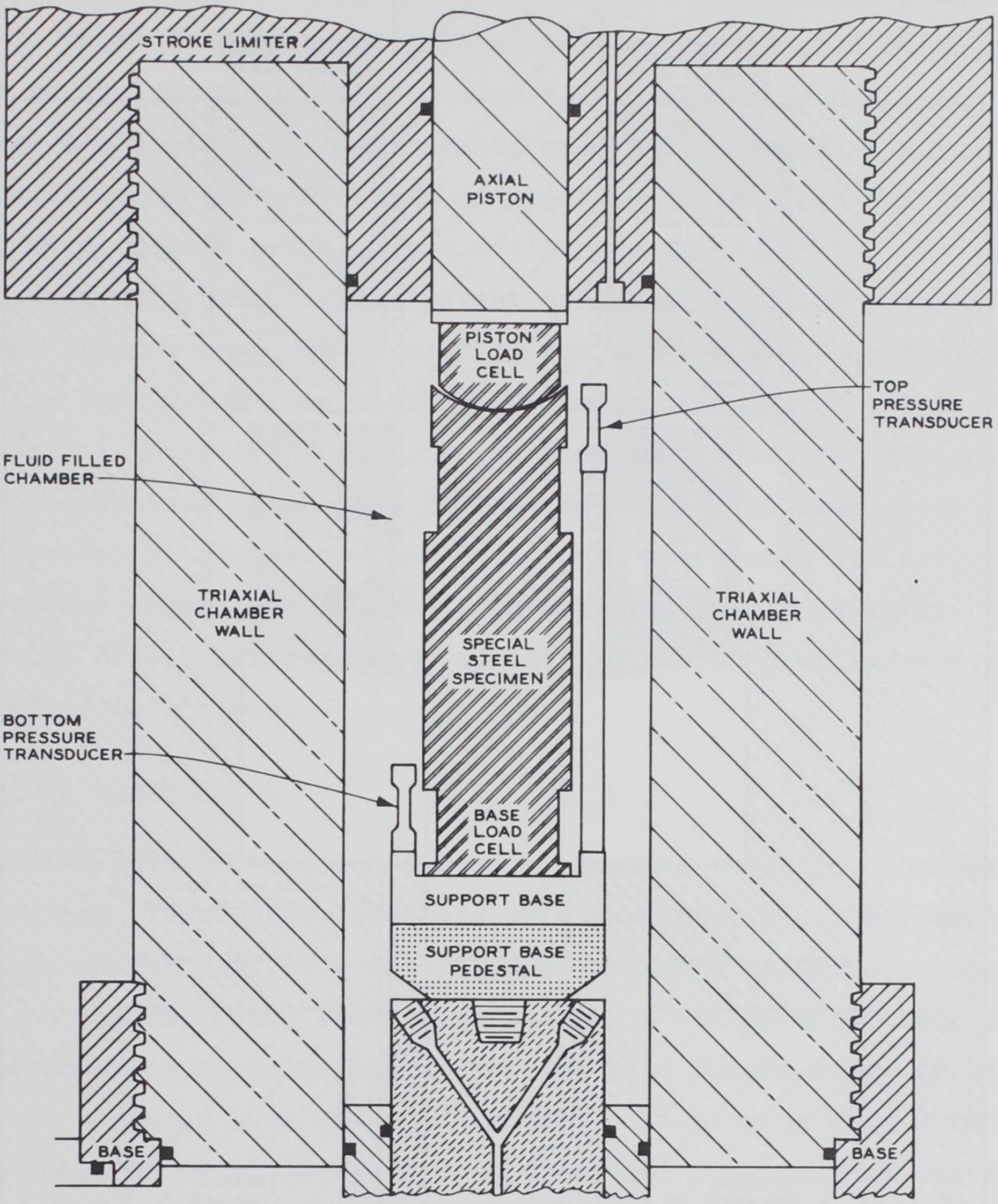

Figure 2.6 Cross section of the triaxial chamber.

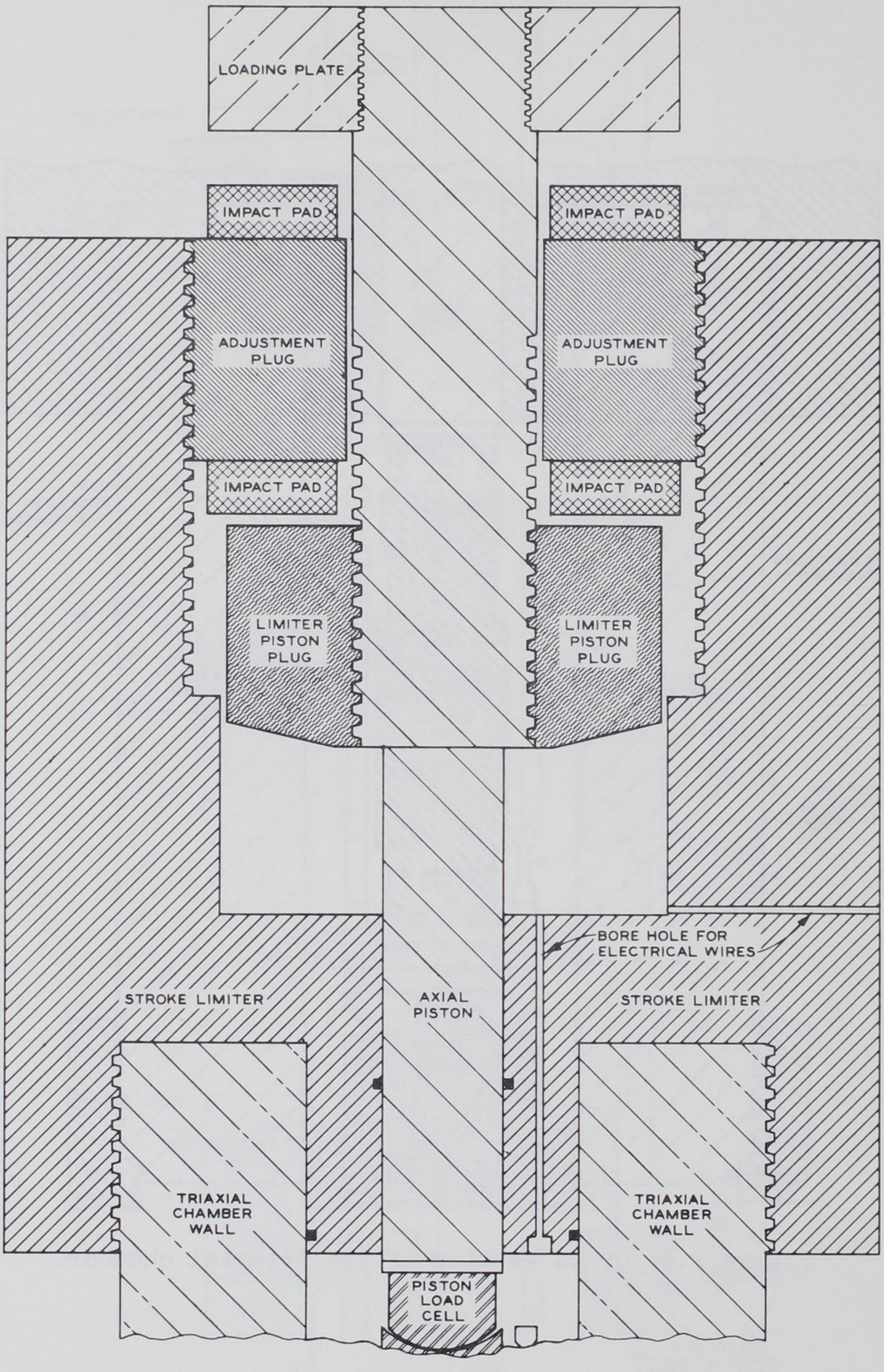

Figure 2.7 Cross section of the stroke limiter.

CHAPTER 3

MEASUREMENT SYSTEM

Time histories of the applied loadings and the specimen's deformation response to those loadings are measured inside the triaxial chamber within the pressure environment. Both commercially available and WES-fabricated transducers are used. The measurements made and recorded as a function of time throughout the tests are chamber pressure, axial load delivered to the specimen, axial piston travel, specimen's height deformation, and specimen's diameter deformation. To prevent disturbance of the electrical signals of the transducers, oil is used as the chamber fluid. Since all measurements are made within the chamber, hermetic terminal seals are used to make electrical connections from inside the chamber to the outside. A set of nine four-terminal connectors is located around the base pedestal and six single-terminal connectors are located in the stroke limiter. The output from the several transducers, in addition to timing marks, is recorded with a direct-writing, high-speed, light-beam oscillograph with a paper speed of 160 in/sec.

3.1 PRESSURE MEASUREMENT

There are several techniques used to measure pressure, such as strain-gaged diaphragm transducers, piezoelectric crystals, etc. All techniques were considered for use. The selection of suitable transducers for the DHT was based on the following requirements: (1) A standard physical size to allow interchanging of units having intermediate ranges of up to 15,000 psi. Since it was believed that one unit capable of measuring from 0 to 15,000 psi could not provide the necessary accuracy for low-pressure tests, use of several different sizes would require separate adapters, thereby increasing the fabrication costs. (2) A minimum dynamic response capability of measuring the complete pressure history to peak value in times as short as 3-msec rise time, but also allowing for measurement of static pressures applied over periods of time as long as an hour. (3) A physical size and mode of operation to allow placement of the unit within the chamber and in close proximity to the specimen. (4) Electrical wires carrying the signal

from the unit to the recorder that do not require any special insulation. (5) A unit that would be compatible with existing recording systems and would allow for in-place calibration.

The pressure transducer was a WES-designed and fabricated small thin-wall cylinder, sealed at both ends and strain-gaged at midheight. The strain gages were 1/8-inch, 120-ohm, metal-foil gages. As pressure is applied to the unit, the strain gages monitor the deformation of the cylinder walls. The pressure range of the unit is controlled by the cylinder wall thickness, or more specifically, since the external dimensions are fixed, by the internal bore of the unit. Figure 3.1a shows one such unit. The threaded male portion at the base of the unit is used to attach the unit to the holding ring, which will be discussed later. A diagram of the electrical circuit is shown in Figure 3.1b.

3.2 LOAD MEASUREMENT

Requirements similar to those for pressure measurement units were used to select the load measurement transducers. Experience with the WES static high-pressure triaxial device indicated that a strain-gaged solid cylinder design should be used for the DHT. The loading range of a particular load cell was determined by the cylinder diameter. Two load cells were used. One was attached to the axial load piston inside the chamber, and the other was incorporated in the specimen's base pedestal. The use of two load cells, located at both ends of the specimen, allowed monitoring of the dynamic loads to determine if the test material was being loaded too fast, a condition that would produce a nonuniform load distribution within the specimen.

Two separate configurations were selected, one for the piston load cell and the other for the base load cell. The piston load cell has a threaded end to allow attachment to the axial loading piston and a rounded end to mate with the specimen's top cap to allow load transfer to the specimen. One such piston load cell and the corresponding wiring schematic are shown in Figure 3.2. The base load cell consists of a threaded portion to allow attachment to the base pedestal and a flat top portion at the other end upon which the specimen is placed. A typical base load cell is shown

in Figure 3.3a, and Figure 3.3b shows the wiring schematic.

An important consideration in the use of such load cells was the effect of pressure on strain gages and bending of the load cell, which would cause an erroneous output. Techniques of placement of the metal-foil strain gages and optimum electrical circuit design, developed for operation in static high-pressure environments, were adopted for this test device. A maximum output signal of 1 percent of full vertical load output signal, when subjected to only confining pressure, was permissible for each load cell. Periodic calibration checks of each load cell are made throughout its use to insure accurate measurements.

3.3 SPECIMEN DEFORMATION MEASUREMENT

The determination of specimen response to triaxial test loadings requires that both axial and lateral deformation be measured. In tests on stiff, fairly smooth-textured, competent rock specimens, use of strain gages bonded directly or indirectly to the rock's surface has proved satisfactory. Such gages are commonly used for strain measurements. However, in the case of soils and poor-quality rocks, measurements must be made by other means.

The vertical deformeter used in the DHT tests consists of two commercially manufactured linear variable differential transducers (LVDT's) mounted in the holding ring at 180 degrees around the specimen. It monitors movement of the top cap, which is affixed to the specimen. The output from each unit is recorded separately. Calibration of the units is made in place and under pressure. Figure 3.4a shows the two units and their holding ring, which is placed around the specimen. Figure 3.4b is a schematic electrical circuit of one such unit. It should be noted that a film potentiometer mounted outside the chamber monitors the axial piston travel. In those tests in which the piston is in contact with the specimen's top cap (e.g., a shear test), the recorded output of the potentiometer can be used to cross check the vertical deformeter data.

The lateral deformeter consists of three LVDT's, which are mounted horizontally, and is similar to the one used in the study described in Reference 1. Figure 3.5a shows the LVDT's in the holding ring. The device is

calibrated in place as a single unit, and the outputs from the three LVDT units are averaged to produce one recorded output that denotes an average diameter change. The electrical circuit for this device is shown in Figure 3.5b.

Another device was initially used to measure lateral deformation. It consisted of strain-gaged cantilever spring arms, as described in Reference 2, but proved unsatisfactory. A modified design is currently under evaluation for use with large-strain-producing materials.

3.4 RECORDING SYSTEM

The output voltage signal from each of the measurement units is converted by a carrier amplifier into a proportional output current signal, which is used to operate galvanometers that record the data on light-sensitive paper. A precise kHz signal from an oscillator is used to produce 1-msec timing marks on the recording paper. A diagram of the measurement system and the recording system is shown in Figure 3.6, and a detailed discussion of the recording system is presented in Reference 3.

3.5 SPECIMEN PLACEMENT PROCEDURE

A special instrumentation package was developed to minimize the time required to disassemble (and subsequently reassemble) the triaxial chamber from the base to allow the installation of a test specimen and measurement system prior to each test. The package consists of a support base, six rods, and the various ring-shaped holding units to which each of the deformeters and pressure transducers is attached. In preparation for a test, the specimen is placed on the base load cell, and the top cap is placed on the specimen. Then a standard triaxial rubber membrane (used to seal the specimen from the chamber fluid) is slipped over the specimen and sealed at the top cap and base. A special rubber compound is painted on the outside of the membrane to prevent deterioration of the membrane by the chamber oil. Three rods are then placed around the specimen and fastened to the support base. The deformeter holding rings are slipped over the rods, located at the desired height of the specimen, and fastened to the three rods to prevent movement. The complete package, as shown in Figure 3.7, can then be

lowered into the triaxial chamber and attached by three of the rods, which extend through the support base, to the base pedestal. Electrical connections are made to the hermetic terminal to bring the electrical signals out of the chamber. The chamber is filled with oil, and the stroke limiter is attached. The axial piston is lowered into contact with the specimen top cap by changing the position of the adjustment plug, and the desired allowable piston stroke is set.

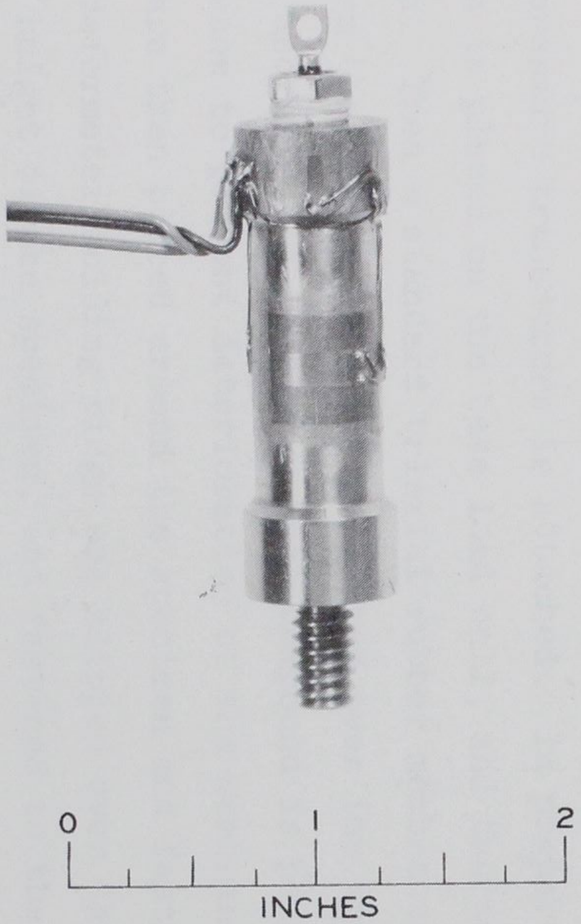

a. WES INTERNALLY MOUNTED PRESSURE TRANSDUCER

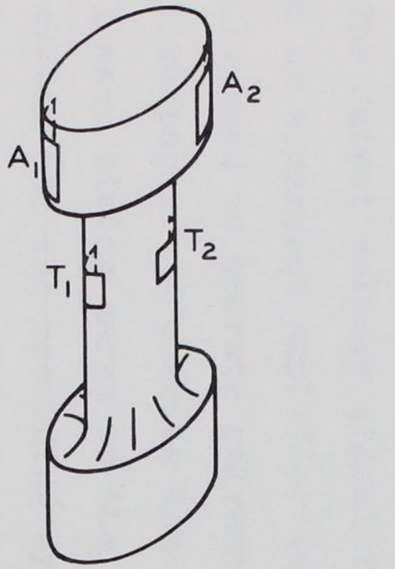

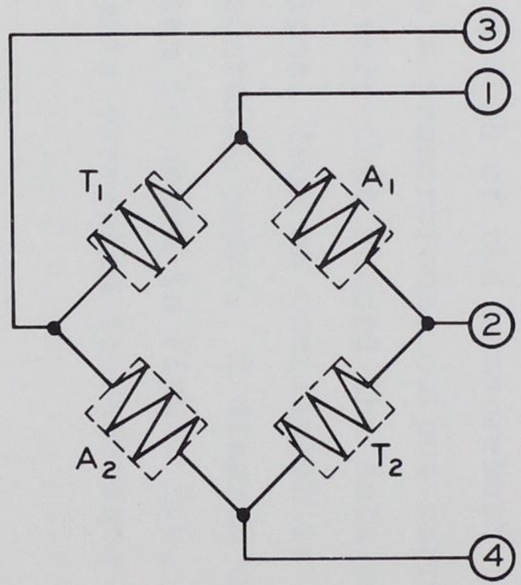

LEGEND

	METAL FOIL STRAIN GAGE
T_1	TRANSVERSELY MOUNTED STRAIN GAGE
A_1	AXIALLY MOUNTED STRAIN GAGE

b. WIRING SCHEMATIC FOR PRESSURE TRANSDUCERS

Figure 3.1 WES pressure transducer and wiring schematic.

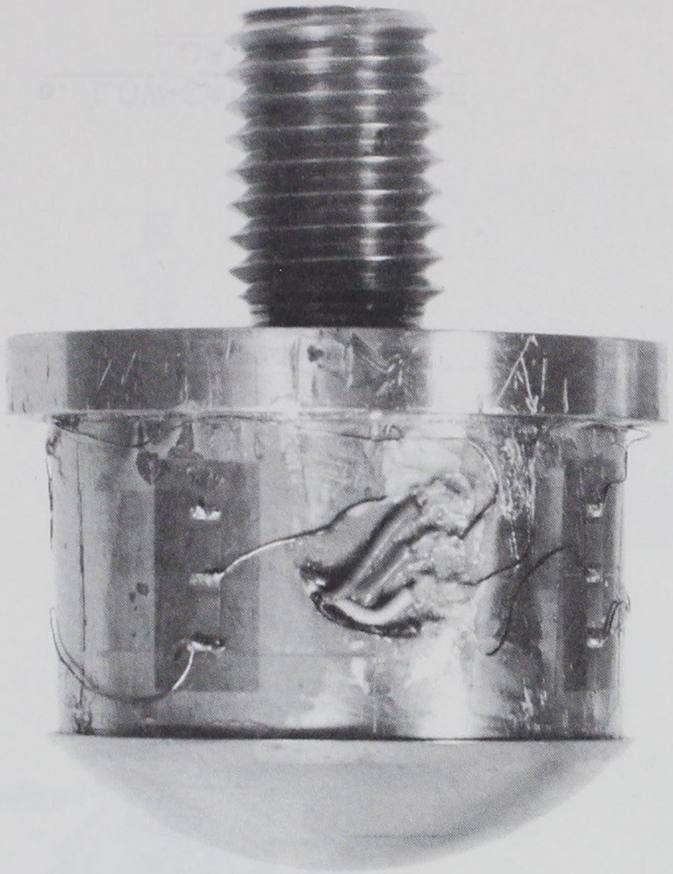

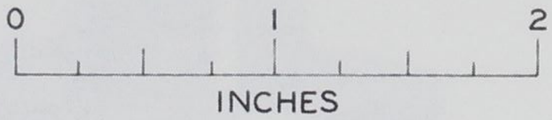

a. HIGH-CAPACITY PISTON LOAD CELL

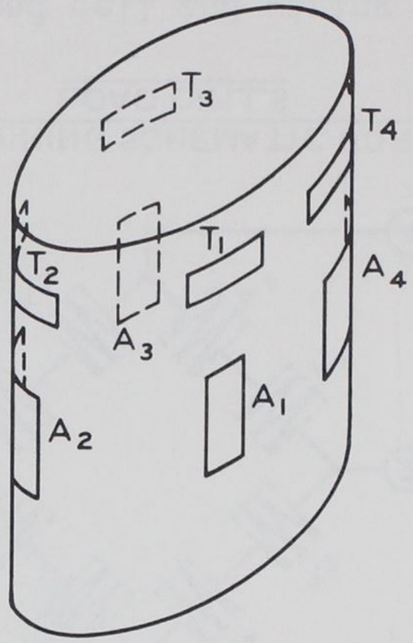

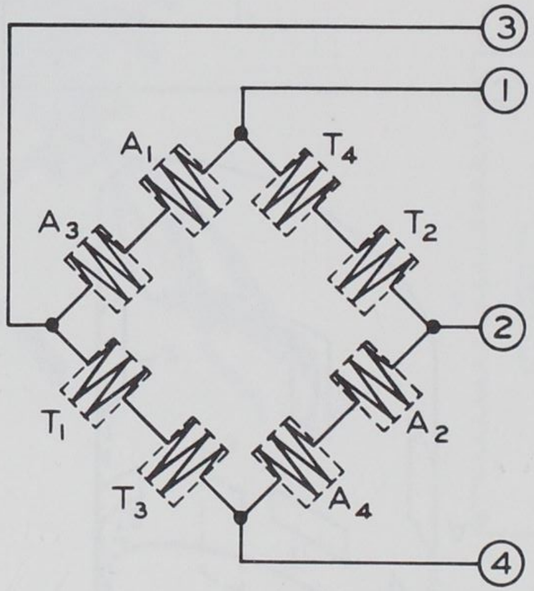

LEGEND

	METAL FOIL STRAIN GAGE
T_1	TRANSVERSELY MOUNTED STRAIN GAGE
A_1	AXIALLY MOUNTED STRAIN GAGE

b. WIRING SCHEMATIC FOR LOAD CELLS

Figure 3.2 High-capacity piston load cell and wiring schematic.

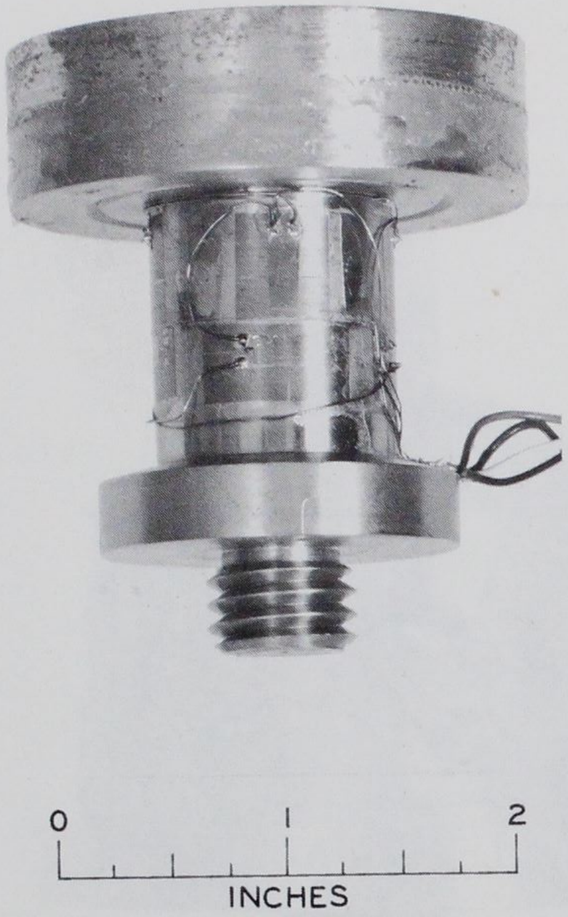

a. LOW-CAPACITY BASE LOAD CELL

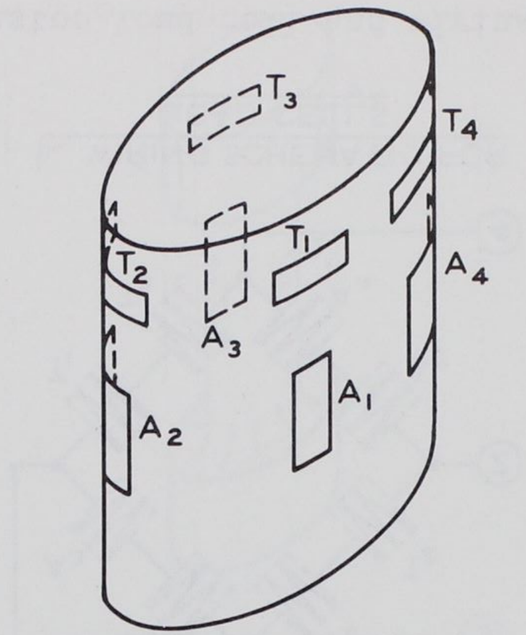

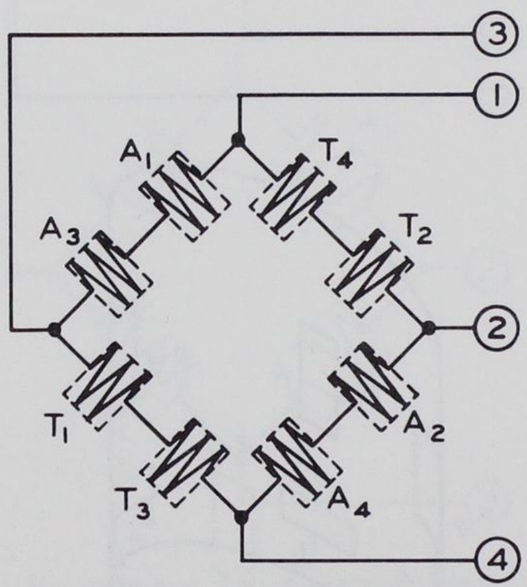

LEGEND

- METAL FOIL STRAIN GAGE
- T_1 TRANSVERSELY MOUNTED STRAIN GAGE
- A_1 AXIALLY MOUNTED STRAIN GAGE

b. WIRING SCHEMATIC FOR LOAD CELLS

Figure 3.3 Low-capacity base load cell and wiring schematic.

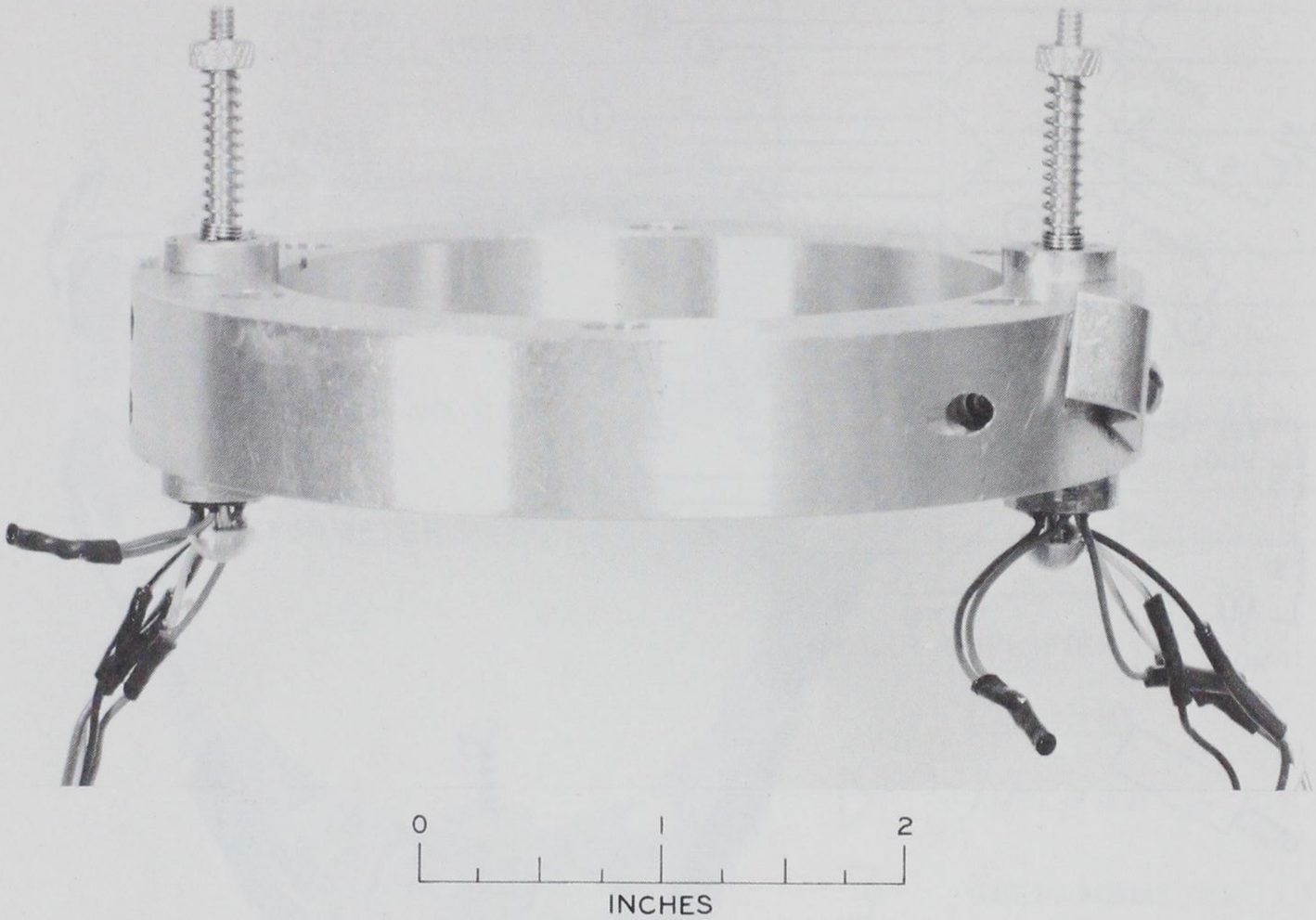

a. VERTICAL DEFORMETER CONSISTING OF TWO LVDT UNITS AND HOLDING RING

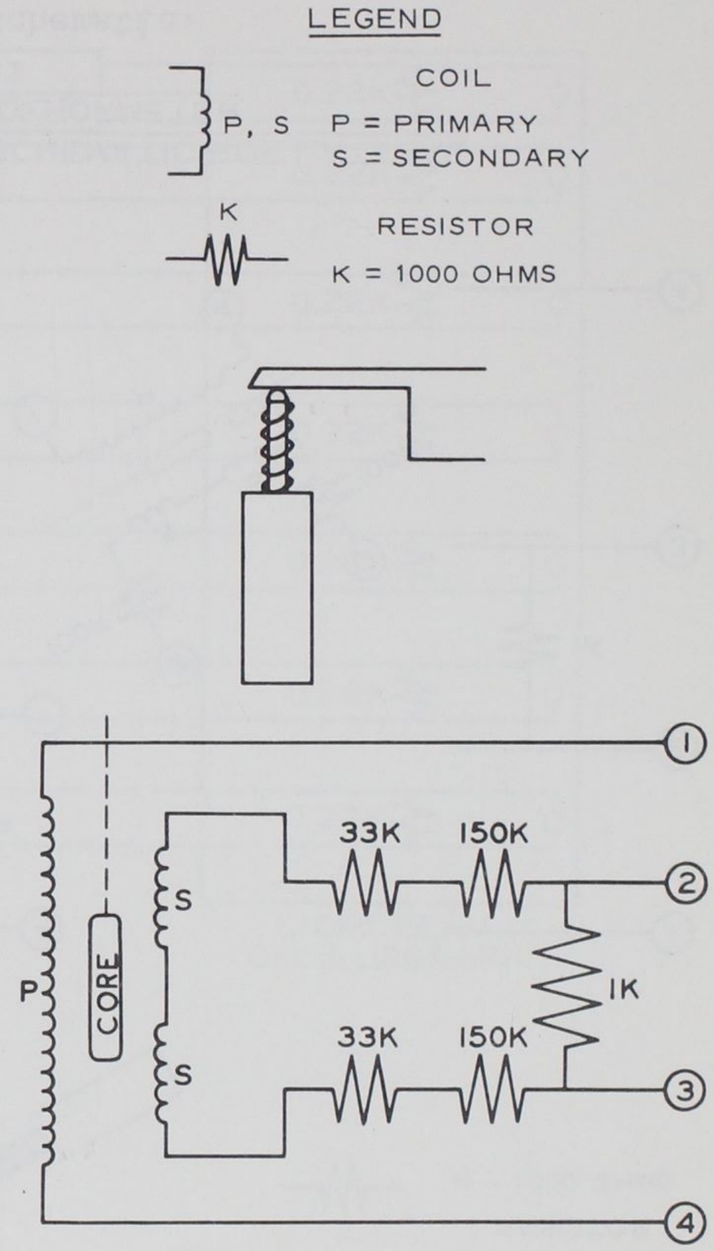

b. WIRING SCHEMATIC FOR VERTICAL DEFORMETERS

Figure 3.4 Vertical deformeter and wiring schematic.

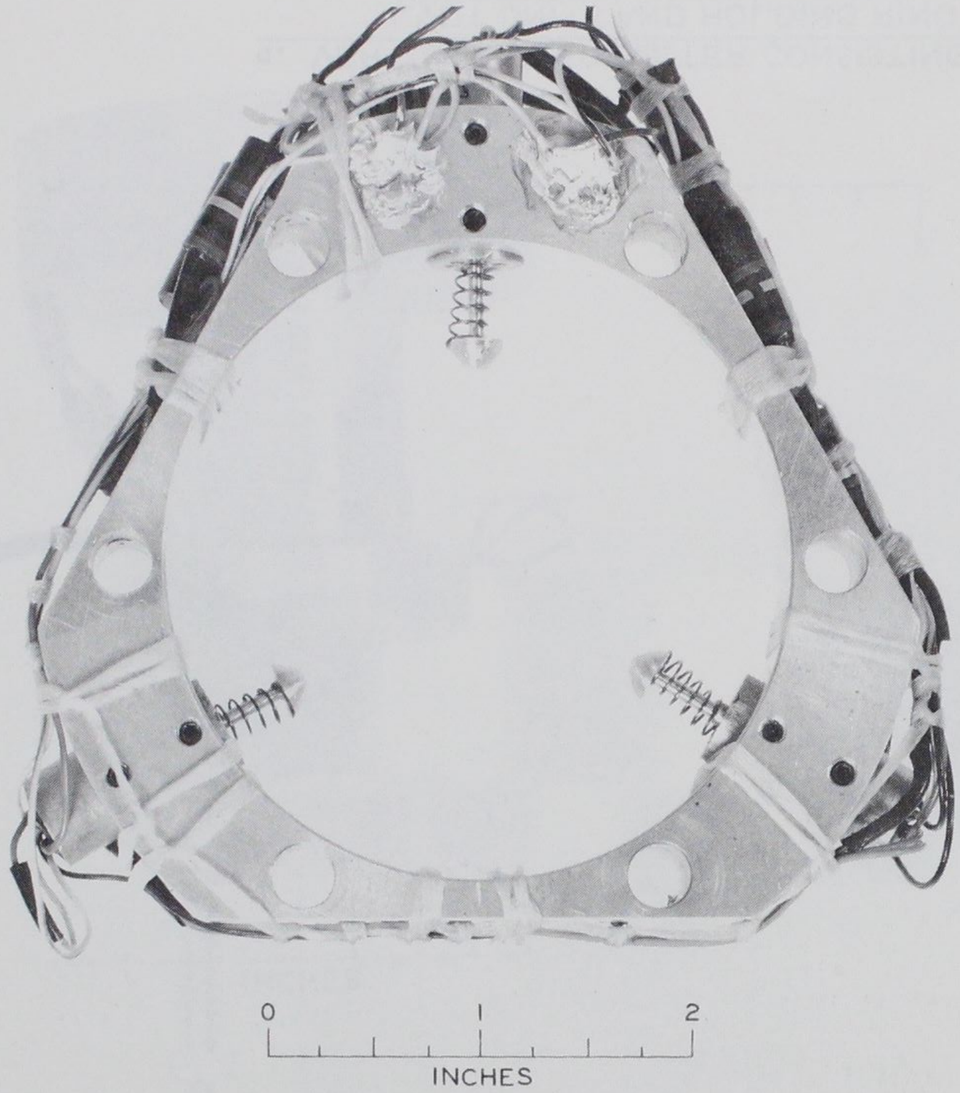

a. THE LATERAL DEFORMETER CONSISTING OF THREE LVDT UNITS AND HOLDING RING

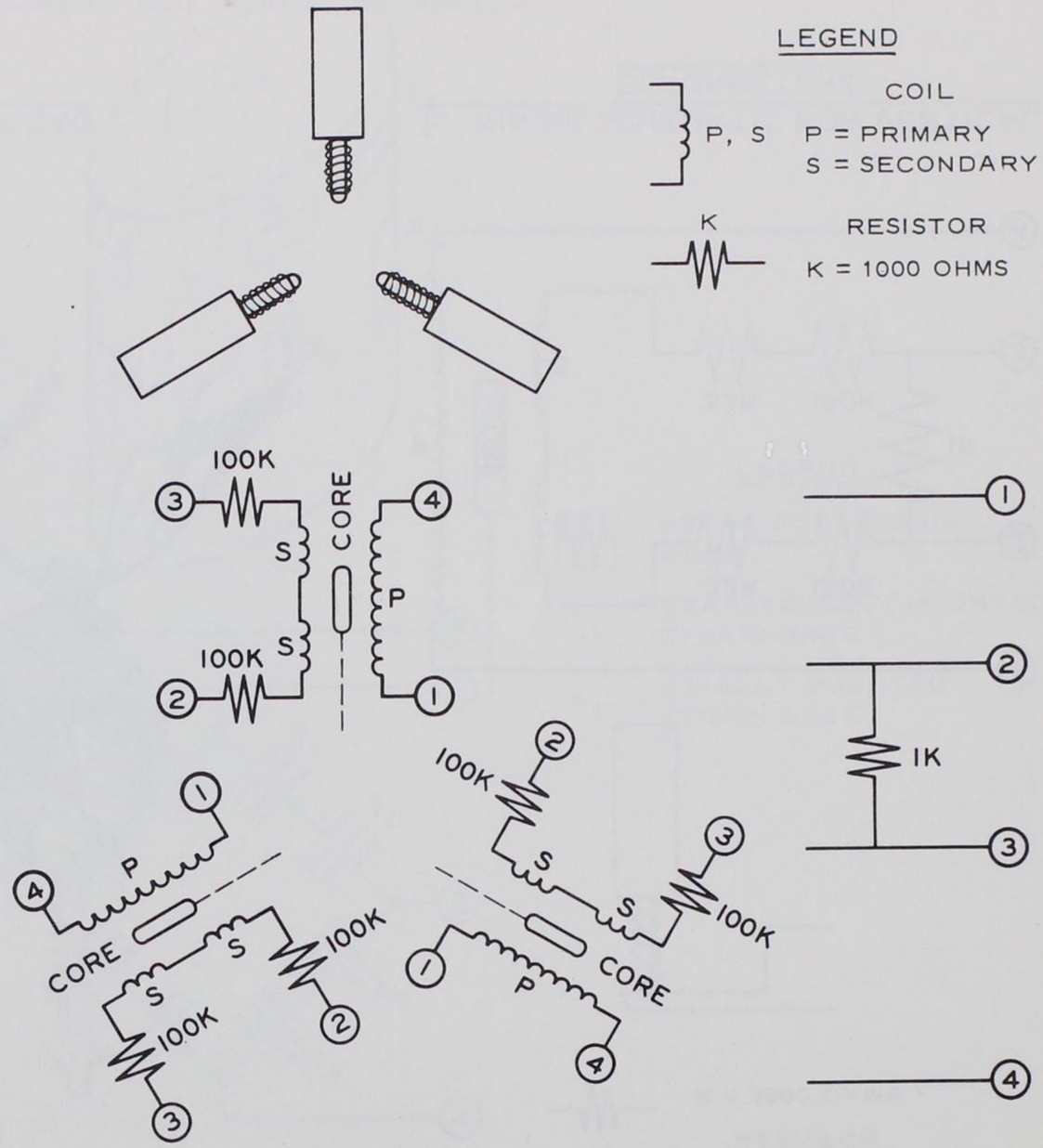

b. WIRING SCHEMATIC FOR LATERAL DEFORMETER

Figure 3.5 Lateral deformeter and wiring schematic.

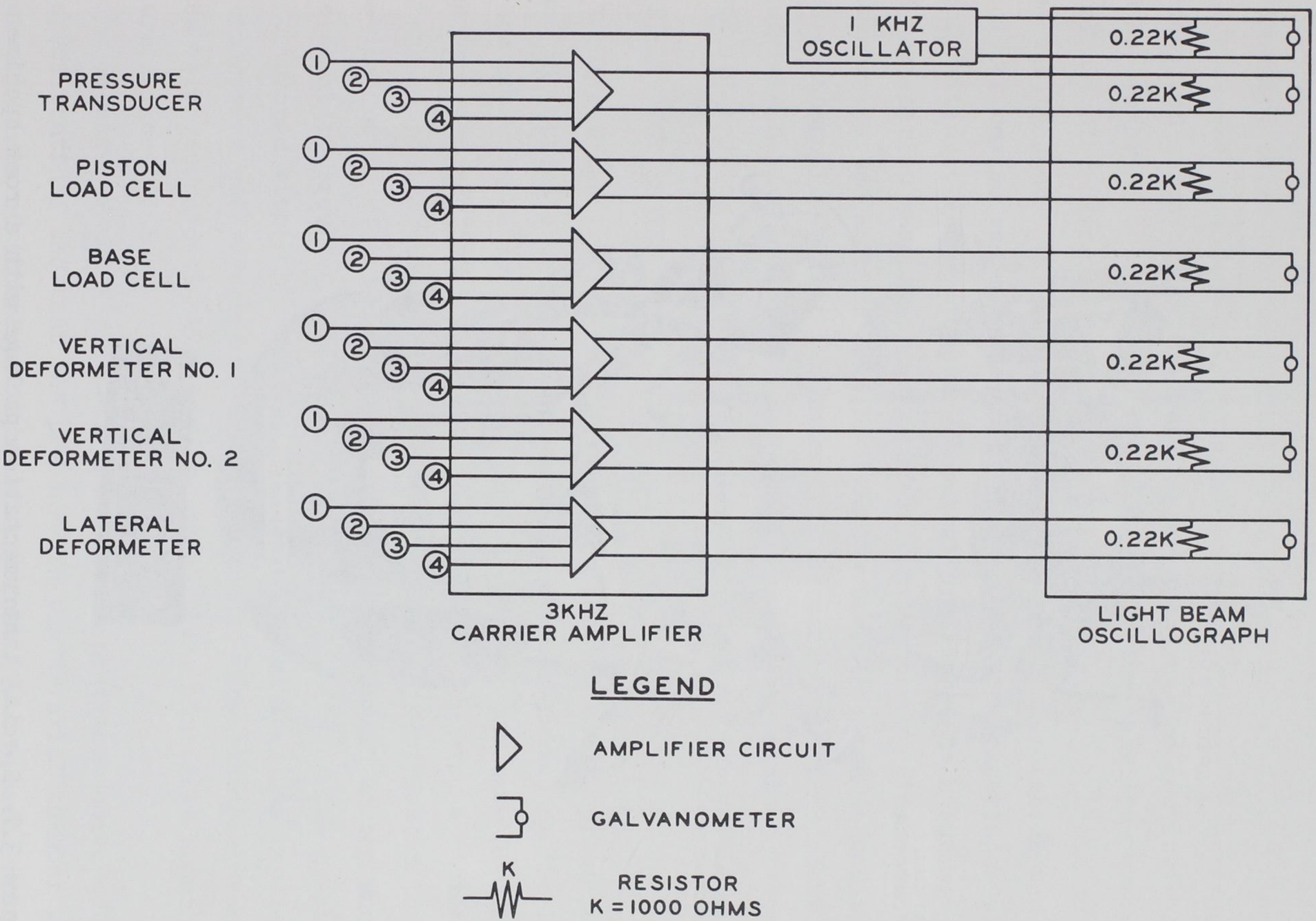

Figure 3.6 Schematic of the electrical circuit for the recording system.

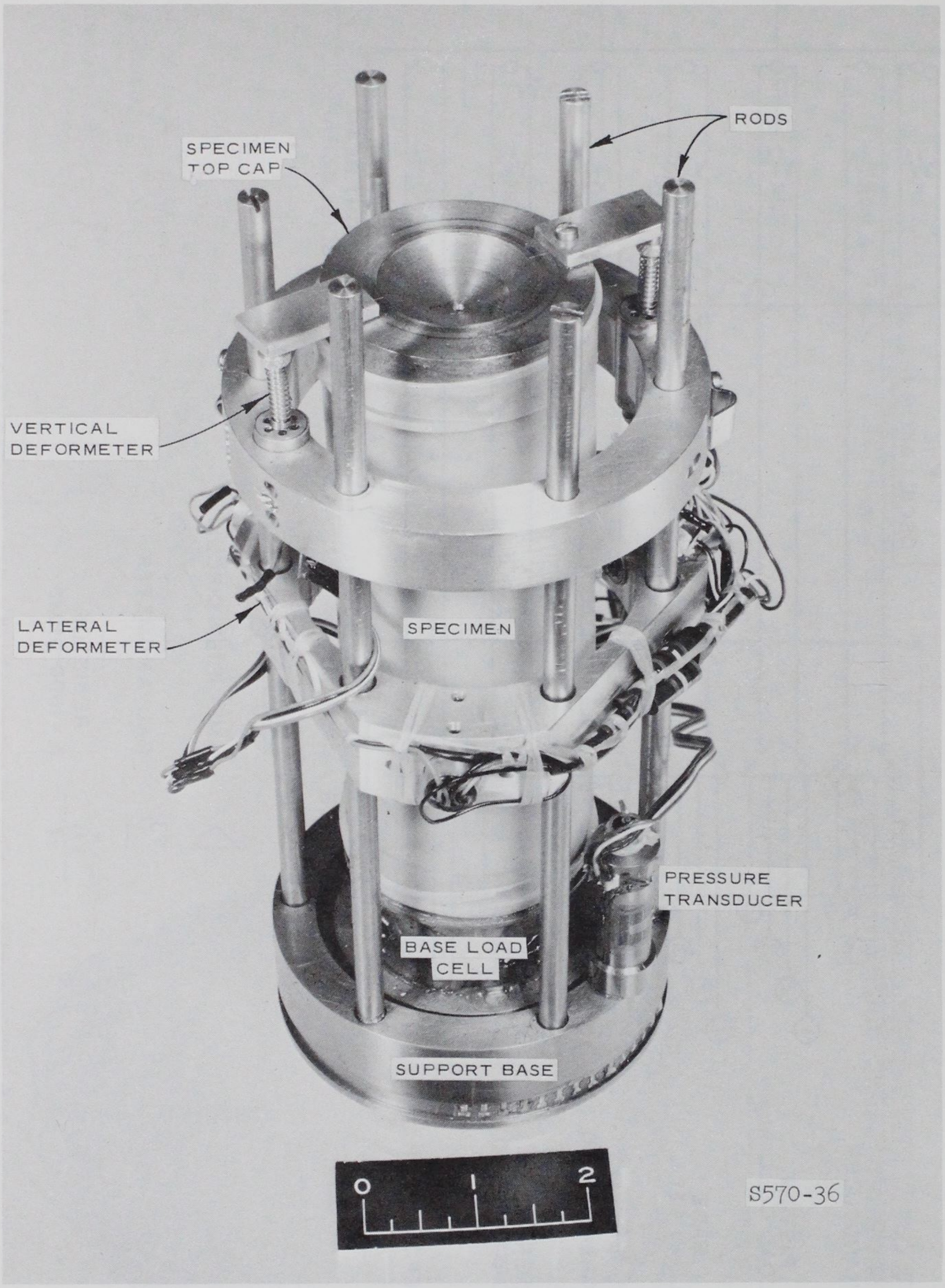

Figure 3.7 Special instrumentation package with a rock specimen in place.

CHAPTER 4

PERFORMANCE TESTS

To date, three test series have been conducted in the DHT. The first test series was performed in connection with the contract proof-test requirement and demonstrated the capability of the device and how well it could be synchronized with the SECO loader. A steel specimen was used in lieu of actual rock or soil specimens for these tests. The second test series was conducted with NX-size siltstone specimens to check the performance of the device and measurement system, to provide experience with the control settings, and to help develop test procedural techniques. The third test series was conducted on NX-size sandstone specimens to evaluate the techniques and methods developed during the first and second test series. Although it was not the intent of the second and third test series to study the behavior of rock specimens under dynamic states of stress, several interesting observations can be made based on the data trends.

4.1 FIRST TEST SERIES

The first test series consisted of two phases, one to proof-test the DHT and the other to determine how well the loading pulses of the DHT and SECO loader could be synchronized. In both phases, the same measurement system was used and consisted of two pressure transducers, a piston load cell, and a special steel test specimen, which was instrumented to serve as a base load cell. The two pressure transducers, mounted at top and bottom of the chamber, provided data regarding the uniformity of the pressure pulse developed within the chamber. Since no axial load was applied, the load cells were not required in the first phase. Nevertheless, their responses were recorded to allow evaluation of their stability under dynamic pressure pulses.

The results of the first test phase showed that the device met all design specifications and that the pressure in the triaxial chamber was uniform at all times of interest. During very fast (3 to 5 msec) rise times, the pressure did overshoot the desired peak pressure because of anticipated inertial effects and resulted in an oscillation, as typified in the plot of

pressure versus time shown in Figure 4.1. At slower (5 to 20 msec) rise times, when no overshoot occurred, only slight oscillations appeared in the loading pulse. A plot of pressure versus time from such a test is shown in Figure 4.2. Both of these pulse oscillations were expected due to inertia of moving masses and are not considered undesirable since unloading-reloading behavior is obtained from specimens subjected to such pulses. However, one problem area was discovered in the stroke limiter that resulted in an undesirable upward movement of the axial piston during application of the fluid pressure pulse. This upward movement was caused by the rubber impact pad on the underside of the height adjustment plug. The rubber pad was replaced by a wooden pad during the second test phase, and this eliminated the objectionable upward motion.

Synchronization of the DHT and the SECO loader in the second test phase was considered to be successful over the full range of design load-pressure pulses. The pulse characteristics remained practically the same with respect to oscillations. For the purpose of illustrating the combined performance of the DHT and SECO loader, one typical test result will be shown, and an explanation of the procedures used to determine the actual load produced by the DHT and the SECO loader to attain the desired load-pressure pulses on the specimen will be given.

For the illustration test, a pressure of 8 kips/in^2 was to be applied to the chamber fluid at a desired pressure rise time of 160 msec, a pressure dwell time of 0, and a pressure decay time of 30 msec. At 60 msec after initiation of the pressure pulse, an axial load of 24 kips was to be applied with a rise time of 40 msec, then decayed after a 0 dwell time to 12 kips in 56 msec. Just prior to initiation of the fluid pressure decay, the vertical load was to decay from 12 to 6 kips, and during decay of the fluid pressure, the vertical load was to decay to 0 kips. Figure 4.3a shows the desired pressure versus time pulse, and Figure 4.3b shows the desired load versus time pulse. The same time coordinate is used for both plots. To program the actual load produced by the SECO, the effect of the pressure within the DHT chamber acting upward on the axial piston must be considered. For this example, a pressure of approximately 36 kips is required to overcome the upward thrust of the piston caused by the peak

pressure of 8 kips/in^2 within the chamber before any load will be measured at the specimen. Therefore, at any given time the desired load on the specimen (shown in Figure 4.3b) plus the reaction load (shown in Figure 4.3c) required to overcome the confining pressure equals the externally applied load delivered by the SECO loader. Figure 4.3d shows the externally applied load required to produce the desired vertical loading pulse on the specimen. In this case, an externally applied load of approximately 46 kips was required. To produce the desired internal load, a rise time of 56 msec, a hold time of 56 msec, and a decay time of 34 msec were applied by the SECO loader. For this test, the multiorifice control valves were set to produce the following times.

DHT		SECO	
Rise Time:	160 msec	Rise Time:	56 msec
Decay Time:	30 msec	Decay Time:	34 msec

The following settings were used for the electrical counters, allowing 500 msec for the oscillograph to reach desired recording speed. All settings are referred to a common zero time.

DHT		SECO	
Initiate Rise:	0500 msec	Initiate Rise:	0542 msec
Initiate Decay:	0660 msec	Initiate Decay:	0656 msec

Figure 4.4 presents plots of pressure and load versus time showing the actual measured pulses of the pressure and load measured at the steel specimen. The decay portions of both pulses, which have a decreasing rate of decay as zero load or pressure is approached, are typical of those of the devices rather than the idealized decay time of constant rate shown in Figure 4.3. The shapes of the measured decay pulses are also closer to those of decay pulses produced by actual blast loadings in the field. Also, the large oscillation shown in the initial portion of the load versus time plot

was caused by a slapping between the axial piston and specimen top. After application of the fluid pressure, the piston was not in contact with the specimen's top, as has been discussed previously. When the externally applied vertical load overcame the upward thrust caused by the confining pressure, the piston was allowed to impact with the specimen with a partially controlled impulse.

As mentioned previously the necessary gas pressures and the proper multimetering orifice openings for each device were selected based on the calibration plots. The calibration plots for the gas pressure and orifice openings were actually based on theoretical calculations made during the design; during the three test series, some slight adjustments of the calibration plots were required. Therefore, some expected deviation between the desired pulses and the actual test pulses was noted.

4.2 SECOND TEST SERIES

The specimens were field NX-size cores of a tan, soft to moderately hard, clayey siltstone taken at a depth of approximately 260 feet below ground surface from the Brule formation in southeast Wyoming. The cores were of poor quality with irregular sides. The test series was conducted to evaluate the performance of the measurement system and to determine how the DHT and SECO would respond after specimen rupture. A variety of loading pulses was selected and applied to gain additional experience in the operation and synchronization of the DHT and SECO loader. The measurement system used consisted of pressure cells, piston and base load cells, a vertical deformeter, and a spring-arm lateral deformeter. The same 100-kip maximum range load cells used in the first test series were also used in this test series because fabrication of more suitable lower range load cells had not been completed. However, because the purpose of the test was to evaluate device performance rather than to study material behavior, the accuracy resulting from the measurement of relatively low-level loads by a high-range load cell was considered sufficient.

The most significant problem disclosed by the test series was the unsatisfactory operation of the spring-arm lateral deformeter. When the pressure was applied dynamically, the deformeter spring arms apparently

oscillated. It is believed that these oscillations occurred because of the physical orientation of the low natural frequency spring arms with respect to the direction of the pressure wave. (The spring-arm deformeter was replaced by the deformeter incorporating LVDT's, as previously described, during the last half of the third test series.) The results presented in this section therefore include only the axial deflection measurements made on the specimens.

It was also discovered during this test series that the load cells reported a negative load and the vertical deformeter reported a corresponding height increase during initial application of confining pressure and during those tests in which the axial load was decayed before removal of the confining pressure. Since application of the confining pressure or complete decay of the axial load would result in a slight upward travel of the axial piston, it appeared as if the specimen's top cap stayed in contact with the piston load cell rather than with the specimen. However, both load cells reported the same negative amount of load. Since a rubber membrane was the only connection between the cells, it was felt that further investigation was necessary to obtain a satisfactory explanation. Next, a limestone specimen with axially mounted strain gages on its surface was tested. The normal test configuration was used, and several tests were conducted with the confining pressure held constant and the load dynamically applied and released. Static check tests were also made. In no case was the load level higher than approximately 50 percent of the specimen's yield strength, and no negative loads were recorded. In the dynamic tests, negative loads were recorded, and the strain gages mounted to the specimen indicated a height increase.

Since the piston load cell used had the same diameter as the top cap, it was surmised that the confining pressure did not have time to get between the piston load cell and top cap. As a result, the pressure acted only in the lateral direction of the piston load cell, top cap, specimen, and base load cell, causing an extension (by the Poisson effect) of the "apparent" continuous column. Because the piston had a slightly larger diameter than the load cell and because the apparent column could not support a tensile load, once the pressure was of sufficient magnitude to

overcome the reaction force, the piston load cell and top cap separated. This allowed the confining pressure to once again act in the axial direction on top of the specimen and under the axial piston. Calculations of strain that would exist under a condition of greater lateral than axial loading verified the strain-gaged load cell's measured output. Also, use of a smaller diameter piston load cell resulted in elimination of the extension loading.

The extension loading condition does provide a unique opportunity for investigating material behavior under dynamic negative deviator stress loadings. Although the levels produced are not sufficient to cause failure in most rock materials, qualitative initial stress-strain data can be obtained. However, it is felt that since the vertical deformeter monitors only top cap movement and there was no way to verify complete contact between the cap and specimen, a better measurement system must first be developed to insure more accurate axial deformation measurements. Also, since the load cells cannot be calibrated under such loadings, the accuracy of the stress value is presently limited to theoretical calculations of load based on the output from the strain gages and assumed stresses on the cell.

The results of four of the tests conducted during the second test series (Tests 2.1 through 2.4) are shown in Figures 4.5 through 4.8, respectively. The measured time-history plots of pressure and load pulses are shown in the upper portion of each figure. A corresponding stress path plot of deviator stress ($\sigma_a - \sigma_r$) versus mean normal stress $\left(P = \frac{\sigma_a + 2\sigma_r}{3}\right)$ illustrating the state of stress to which the specimen was subjected is shown in the bottom portion. Figure 4.5 shows the results of Test 2.1, which consisted of application of confining pressure followed by a constant confining pressure shear test. The lines marked by the circled numbers in Figure 4.5a may be used as references to the actual calculated states of stress on the specimen shown in Figure 4.5b at various times during the test. For example, 2 msec after initiation of the pressure pulse, the pressure is approximately 500 psi and the apparent deviator load is approximately -470 pounds at Point 1 in Figure 4.5a. The corresponding state of

stress on the specimen is a deviator stress ($\sigma_a - \sigma_r$) of -150 psi and a mean normal stress $P = \left(\frac{\sigma_a + 2\sigma_r}{3}\right)$ of 450 psi, as shown in Figure 4.5b at Point 1. At Point 2, the pressure has dropped to 250 psi, and the deviator load has returned to zero. Thus, the deviator stress is 0 psi and the mean normal stress is 250 psi. At Point 3, the confining pressure is 620 psi just prior to axial loading.

From Point 3 to Point 4, the specimen was loaded in 6 msec, unloaded from Point 4 to Point 5, reloaded from Point 5 to Point 6, and finally completely unloaded at Point 7. During the initial loading portion, the confining pressure varied and is reflected in the stress path plot in Figure 4.5b. Point 8 is at the maximum negative deviator stress just prior to piston load cell and specimen top cap separation. The pressure was then decayed to zero as shown at Point 9. The complete time of the test was 86 msec.

The results of Test 2.2 are shown in Figure 4.6. The confining pressure was first applied with a rise time of 6 msec and some overshoot of the pressure occurred (Point 2). The confining pressure started to decay 1 msec prior to application of the axial load. It was intended that the pressure decay at the same time and at the same rate at which the axial load was applied in order that a constant mean normal stress could be maintained; however, the actual loading stress path that resulted is shown in Figure 4.6b (Point 3 to Point 4). The load applied was sufficient to cause specimen failure. Therefore, most of the unloading (Point 4 to Point 5) was not due to load decay (the load column was still compressing the soil specimen), but to the specimen's decreasing ability to take load after failure. Actual load removal occurred 38 msec after the start of the test. The deviator stress did not become negative after load decay because the confining pressure was also near zero.

In Test 2.3, as shown in Figure 4.7, the pressure was applied with a rise time of 20 msec. However, during the first 4 msec of this test, as in the other three, the specimen was subjected to a negative deviator stress loading (Point 1), rather than to a pure hydrostatic loading. At 20 msec, a deviator stress loading was applied under conditions of approximately

constant mean normal stress. At Point 4 the specimen's ultimate strength was reached. Although additional external load was still being applied, the specimen's ability to take load decreased except for the unloading-reloading cycle at Point 5, which was caused by a loading oscillation. Load decay actually was initiated approximately 40 msec from the start of the test. At Point 7, pressure decay was initiated, and maximum negative deviator stress was reached. The pressure reached zero at Point 8, or 104 msec after the start of the test.

The specimen in Test 2.4 was subjected to a pressure of approximately 2,900 psi followed by a deviator stress loading under conditions of constant confining pressure, as shown in Figure 4.8. The pressure was applied in 15 msec and held for 29 msec prior to the shear phase. The oscillations that occurred in the pressure pulse during the pressure application were extremely valuable for obtaining specimen response for both loading and unloading-reloading stress conditions. A similar unloading-reloading in the axial load occurred during the shear phase prior to reaching the specimen's ultimate strength, which was reached at Point 6. Following complete load decay, the pressure was removed in 28 msec.

Although this test series was conducted primarily to study equipment rather than material performance, deviator stresses and axial strain were calculated from the shear phase of each of the four tests. A comparative plot is presented in Figure 4.9. The difference in specimen response between the four tests is attributed to core quality and slight differences in physical properties. It is interesting to observe the general shape of the complete dynamic stress-strain curve. The response is similar to those stress-strain plots of other materials tested in a stiff machine under static conditions (Reference 4). The negative deviator stress portions of the curves following unloading are shown as dashed lines because separation between the top cap and specimen, which may have occurred, would invalidate the axial deformation measurements.

4.3 THIRD TEST SERIES

The third test series was conducted on field NX-size cores of a yellowish tan, hard, Cretaceous sandstone. The sandstone, ranging from medium

to coarse grained, was taken from the Kootenai formation in central Montana at a depth ranging from 70 to 80 feet. The cores were of good physical quality. The measurement system used was similar to that used in the second test series except a lower range and smaller diameter piston load cell was used. Use of the smaller diameter load cell eliminated the negative deviator stress loading because of the area difference between the specimen's top cap and piston load cell, which allowed the confining pressure to act between the piston and top cap. Also, several tests were conducted with the LVDT lateral deformeter, which allowed measurement of lateral deformation of the specimen. Results of four of the tests, tests 3.1 through 3.4, are presented in Figures 4.10 through 4.13, respectively, showing the measured pressure and loading pulses, the measured deformation of the specimen, the calculated stress path, and the calculated deviator stress-axial strain plots. For two tests, 3.3 and 3.4, in which lateral deformation was also measured, the calculated pressure-volumetric strain plot corresponding to the initial hydrostatic loading of the specimen and the calculated deviator stress-deviator strain plot corresponding to the shear phase are also shown (Figures 4.12 and 4.13).

Test 3.1 was conducted on a sandstone specimen containing oxidized zones. Figures 4.10a and 4.10b present the pressure, load, and height deflection plotted as a function of time. The calculated stress path is shown in Figure 4.10c, and the deviator stress versus axial strain plot of the shear phase is shown in Figure 4.10d. The scale used for deviator stress in both of the latter plots is the same so that determination of the mean normal stress at any point on the stress-strain curve can be made. Determination of the time at any point of interest can be made by a process similar to that explained in the discussion of the second test series. For example, the shear phase began 16 msec after initiation of the test. At this time, the mean normal stress of the specimen was 1,200 psi, and the deviator stress was 0. A peak value of deviator stress of 8,300 psi and a mean normal stress of 3,900 psi were reached 4 msec after the start of the shear phase. Due to some overshoot of the axial load, the deviator stress decreased to 6,300 psi and was held over a period of approximately 40 msec. Decay time of the axial load was 20 msec, followed in 20 msec by

complete removal of the confining pressure over a period of 20 msec.

The same specimen was then subjected to approximately the same pressure pulse, but the axial loading pulse was changed to a slower rise time. The amount of external load was increased to insure specimen failure. The results of Test 3.2 are shown in Figure 4.11. At 30 msec from the start of the shear phase, the specimen reached its maximum strength at 8,500-psi deviator stress and 3,840-psi mean normal stress. Thereafter, the specimen continued to deform as its shear resistance decreased to a deviator stress of 4,700 psi 48 msec from the start of the shear phase. The actual unloading or decay time was 15 msec to zero deviator stress. It is interesting to note that the loading portion of the deviator stress-axial strain plot of Test 3.2 indicates that the specimen is only slightly stiffer than that in Test 3.1.

Test 3.3 was conducted on a sandstone specimen without the oxidized zones that had been noted in the specimens used in Tests 3.1 and 3.2. Lateral deformation measurements were made, and the complete test results are shown in Figure 4.12. The specimen was hydrostatically loaded to approximately 4,500 psi in a rise time of 16 msec. The corresponding pressure versus volumetric strain plot calculated from the axial and lateral deformations is shown in Figure 4.12d. The unloading-reloading cycle that occurred at approximately 1,800 psi resulted in a decreased volumetric strain, which does not agree with measured static test data, and the validity of these data is questionable. Additional study is currently being undertaken to explain the measured response. The specimen was then subjected to a deviator stress loading to 6,500 psi under conditions of constant confining pressure and with a rise time of 12 msec. Then, in order to reduce the mean normal stress, the confining pressure was decayed as additional deviator stress was applied. The specimen's ultimate strength was reached at a deviator stress of 11,250 psi and a mean normal stress of 4,600 psi. This was followed by the postyield response. Unfortunately, in this test as in the next test to be discussed (Test 3.4), premature stopping of the oscillograph resulted in a loss of the record of the last portion of the test.

Test 3.4 was conducted on a silty sandstone, and the results are shown in Figure 4.13. The specimen was first subjected to a hydrostatic loading

of 6,200 psi in a rise time of 20 msec. The pressure-volumetric strain plot (Figure 4.13d) again shows the decreased volumetric strain following an unloading-reloading cycle at approximately 2,900 psi. Also, there was apparently some creep during the pressure hold time of 20 msec since the volumetric strain shows some additional decrease at peak value. The shear phase was to have occurred under conditions of constant mean normal stress; however, the axial load was applied just prior (3 msec) to pressure decay. The actual stress condition to which the specimen was subjected is shown in Figure 4.13c, and the corresponding deviator stress-deviator strain curve is shown in Figure 4.13e.

4.4 FUTURE INVESTIGATIONS

The test data presented herein are typical, and although the purpose of the study was limited in scope, the limited results illustrate the direction that future research should take to answer some of the following questions. To what degree are various materials rate-sensitive with respect to yield strength and moduli data? If the yield strength and moduli increase by some factor over static strength and moduli, does the same factor apply to dynamic unloading-reloading moduli? Does the dynamic yield envelope parallel the static yield envelope? Is the material stress path independent under dynamic loadings? Does the material have the same stress-strain history response to dynamic reloadings as it has to static reloadings? How important is creep in dynamic tests? Are the results seen from specimen postyield response under static conditions valid for dynamic loadings? What influences do the boundary conditions of the triaxial test have on the data obtained under dynamic loadings? The capabilities developed will allow research into each of these questions to provide confidence in the understanding of earth materials subjected to states of impulsive-type stresses.

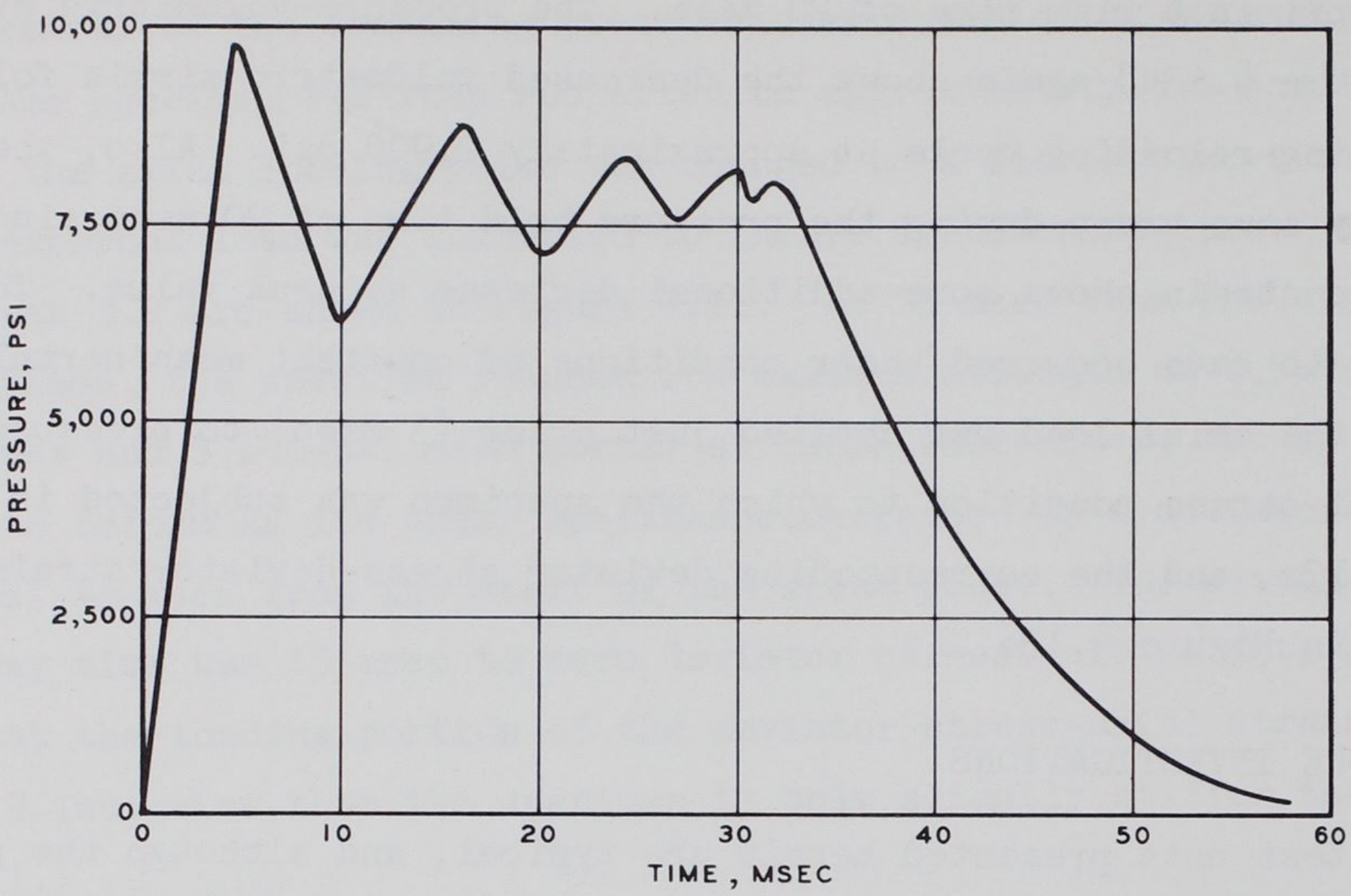

Figure 4.1 Representative pressure versus time plot showing pulse characteristics of very fast rise times.

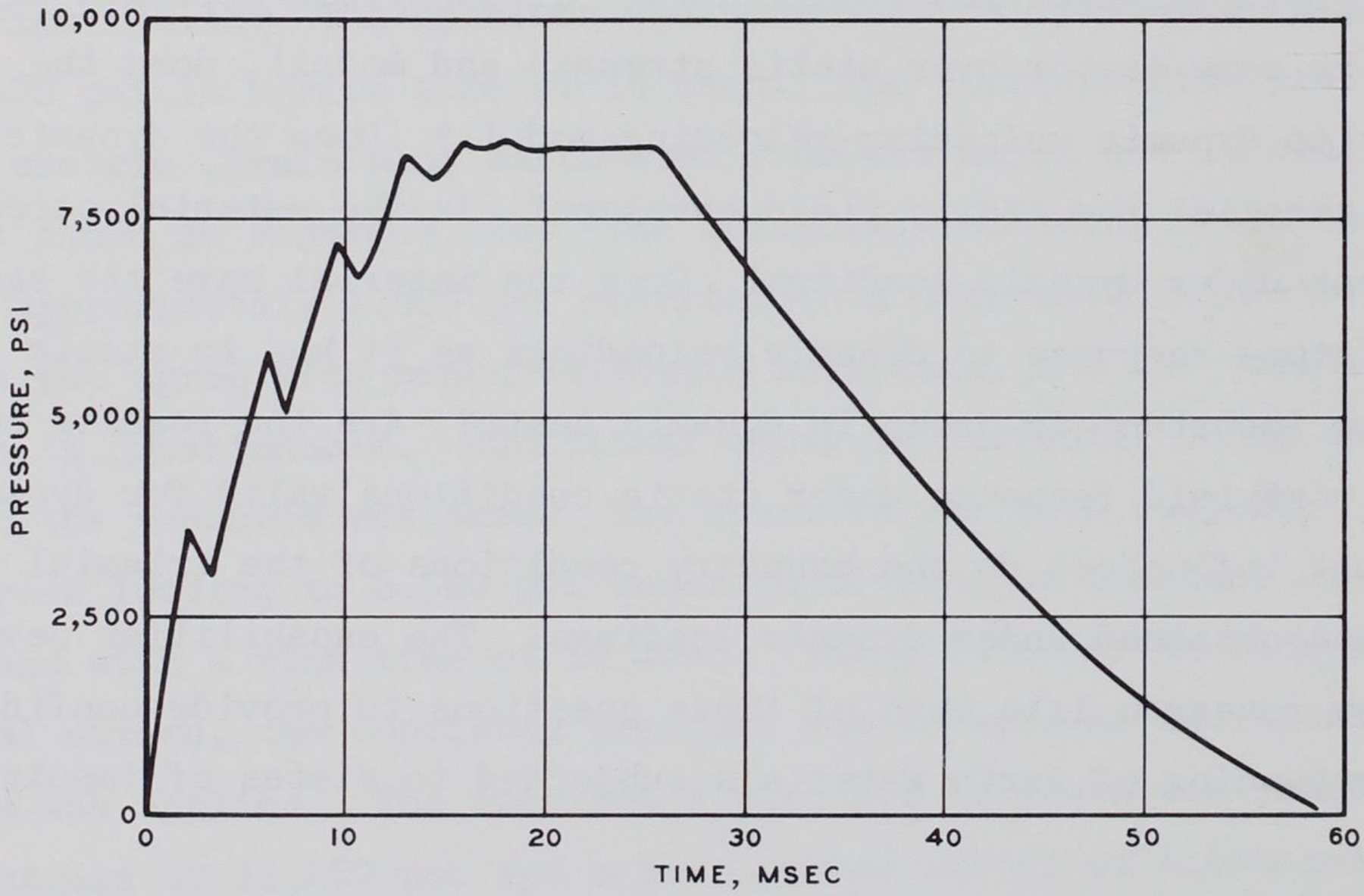

Figure 4.2 Representative pressure versus time plot showing pulse characteristics of moderate rise times.

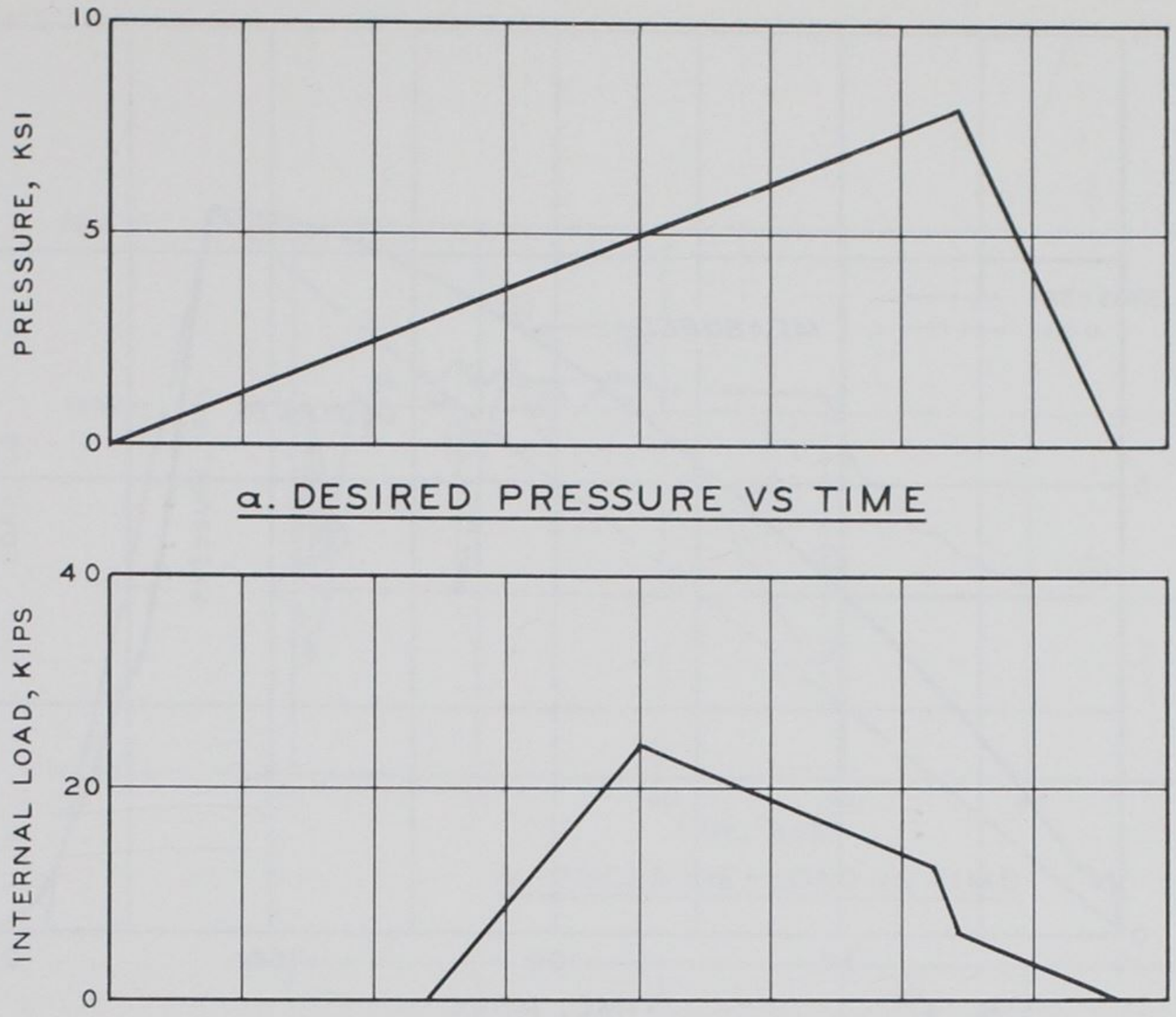

a. DESIRED PRESSURE VS TIME

b. DESIRED INTERNAL LOAD VS TIME

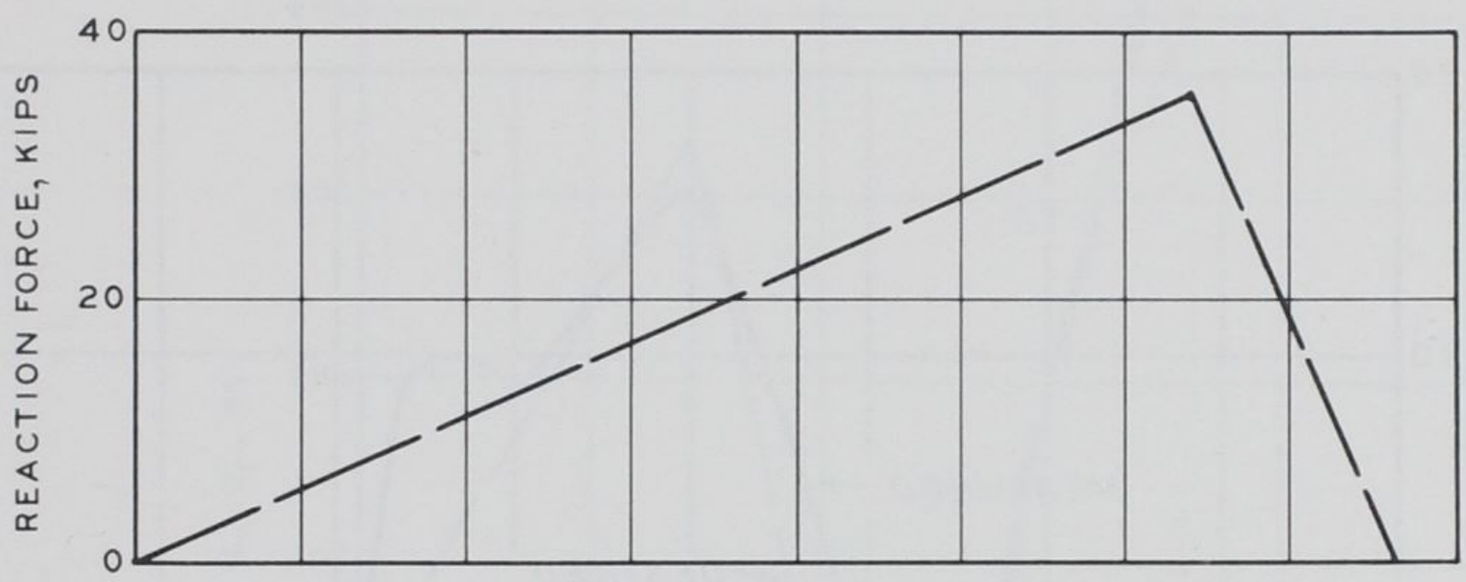

c. REQUIRED REACTION FORCE VS TIME

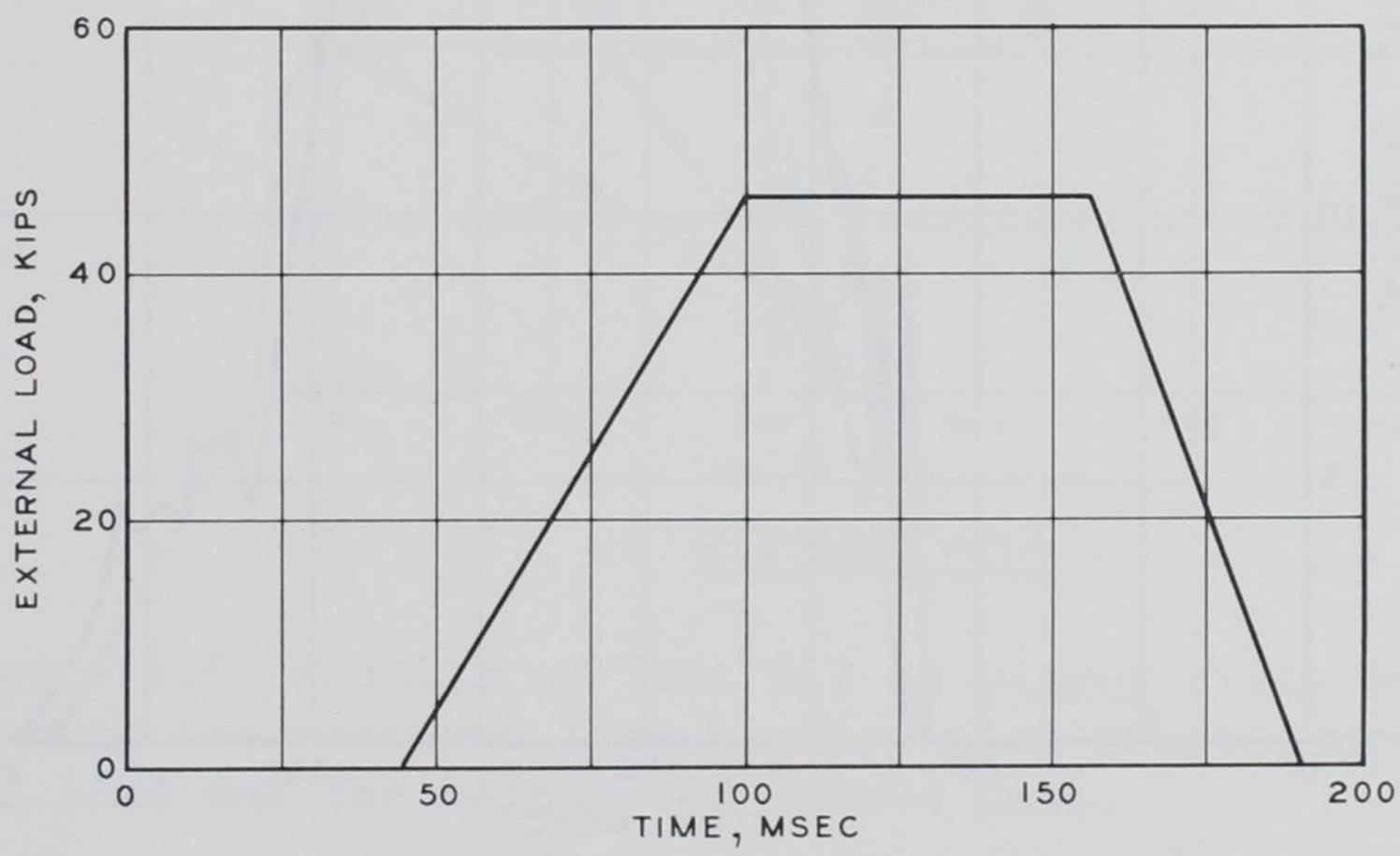

d. REQUIRED EXTERNAL LOAD VS TIME

Figure 4.3 Desired time-history plots of pressure and load used in the determination of control settings.

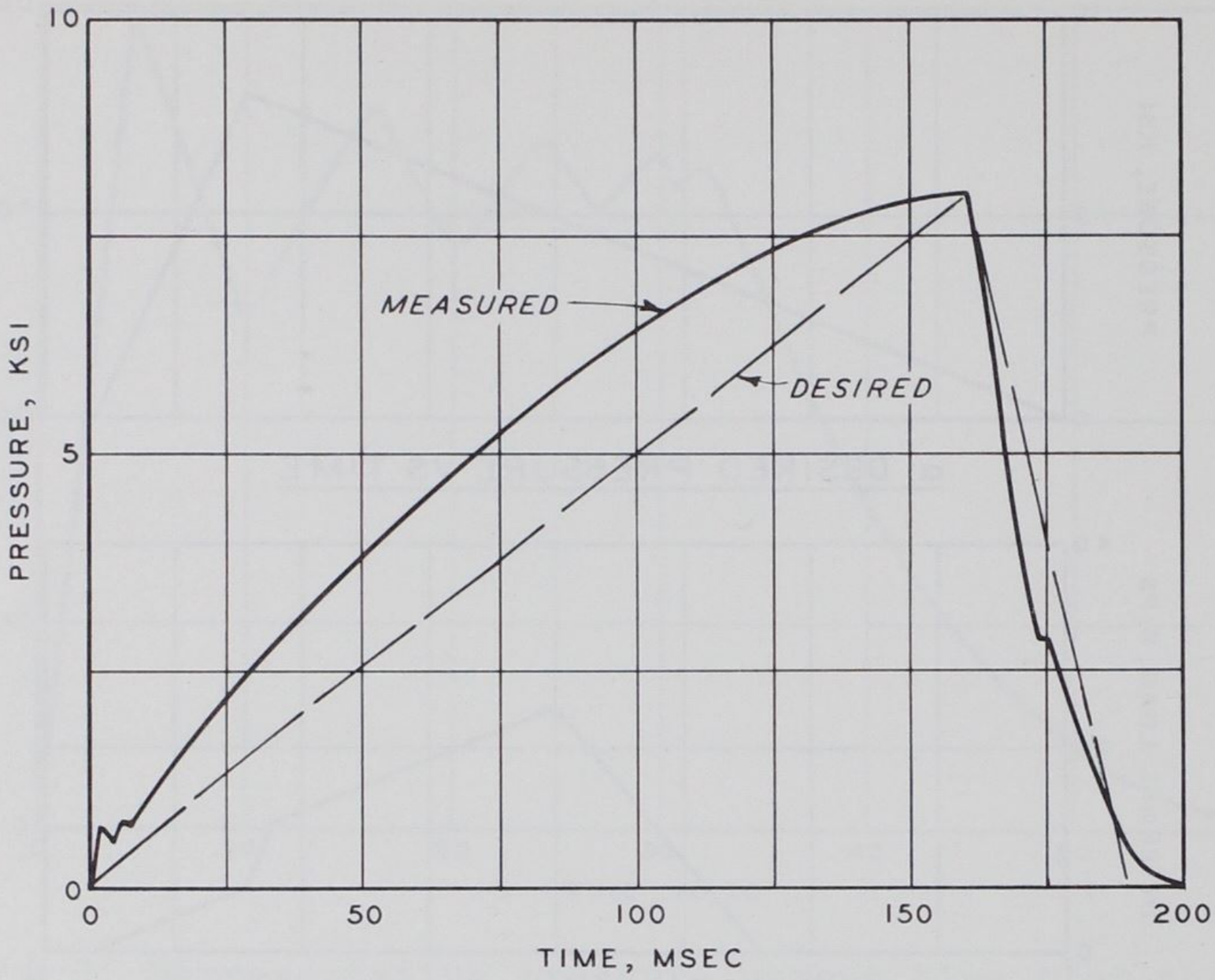

a. PRESSURE VS TIME

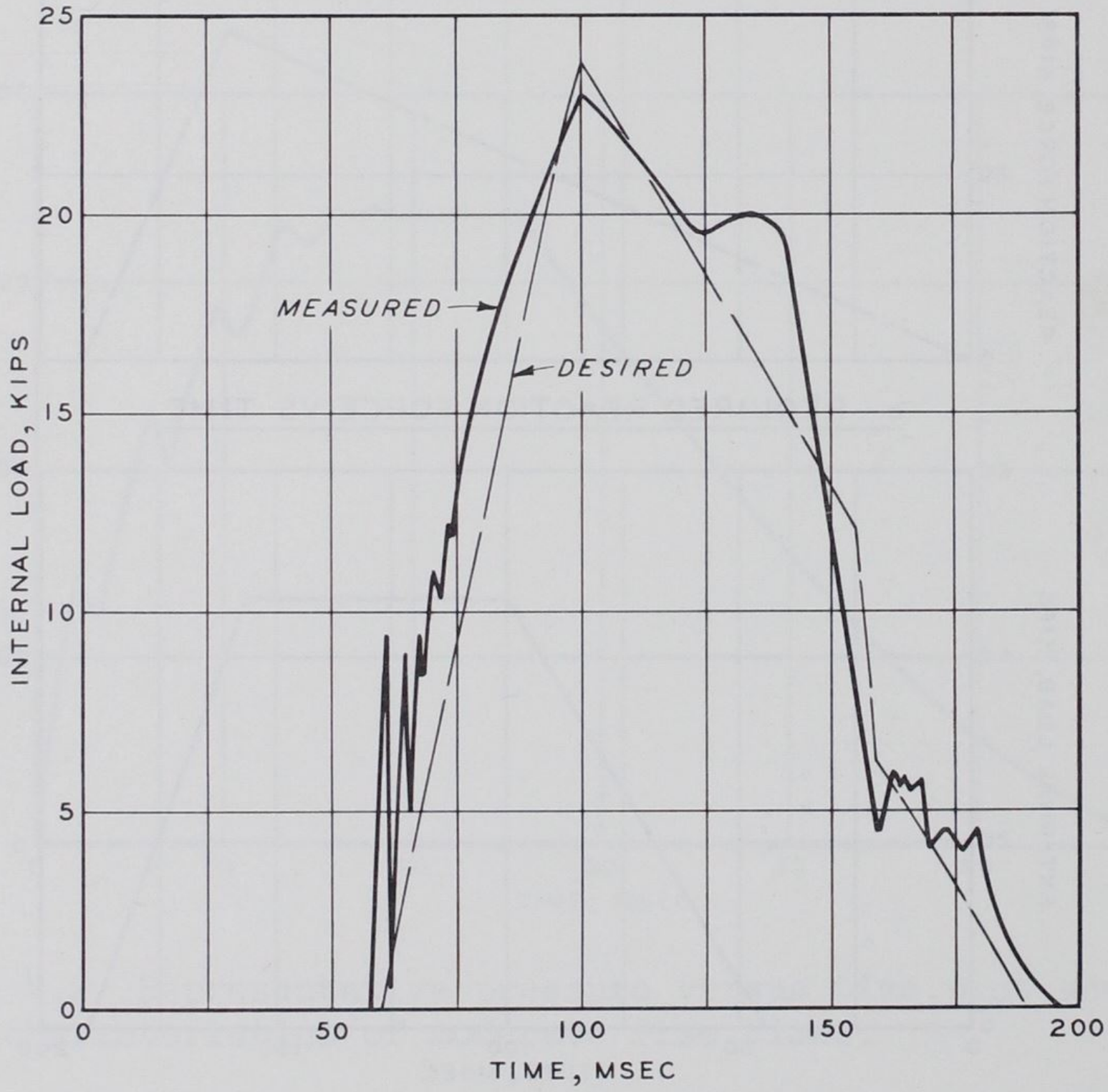

b. INTERNAL LOAD VS TIME

Figure 4.4 Time-history plots of pressure and load based on measured data.

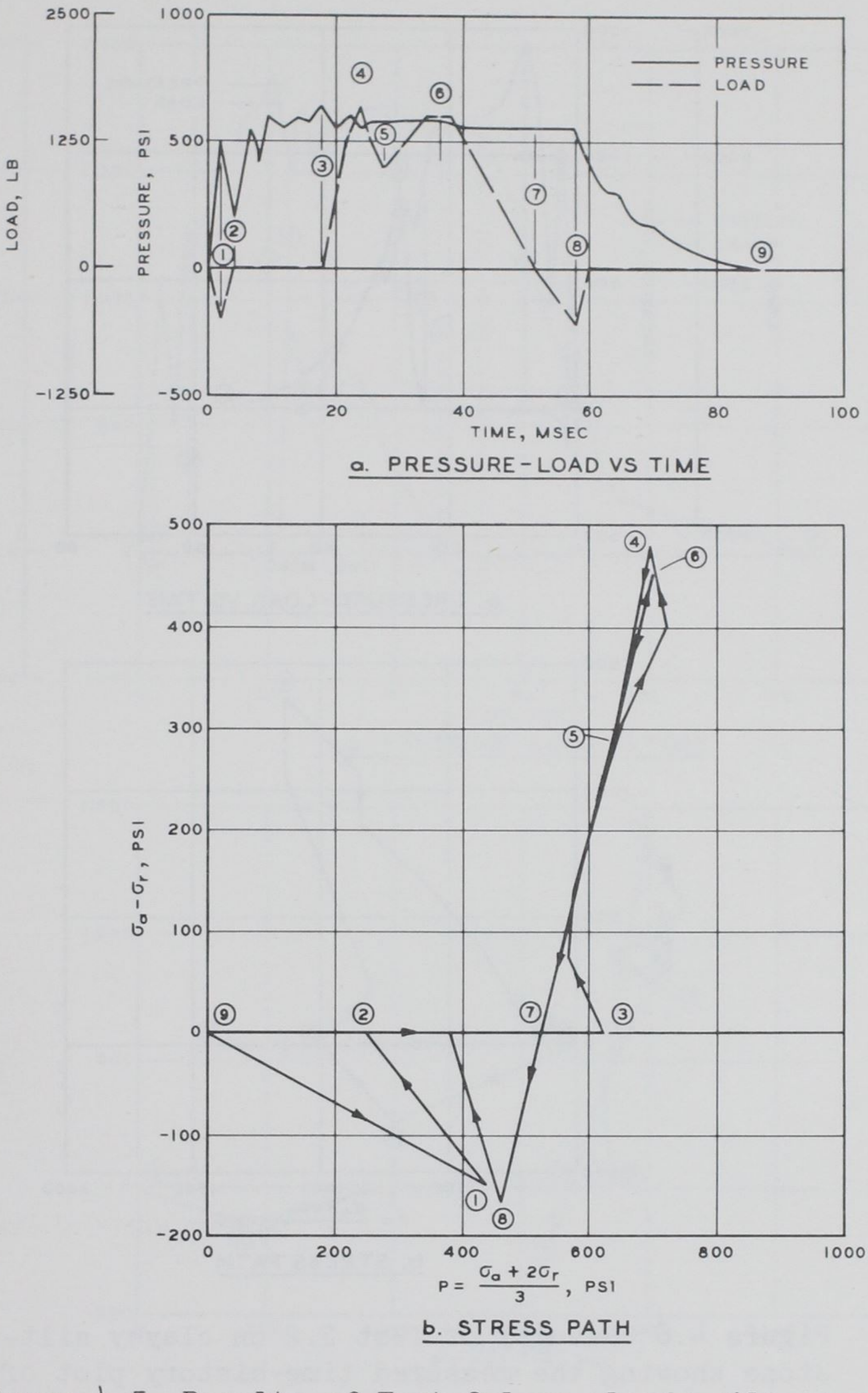

a. PRESSURE-LOAD VS TIME

b. STRESS PATH

Figure 4.5 Results of Test 2.1 on clayey siltstone showing the measured time-history plot of pressure and load and the calculated stress path.

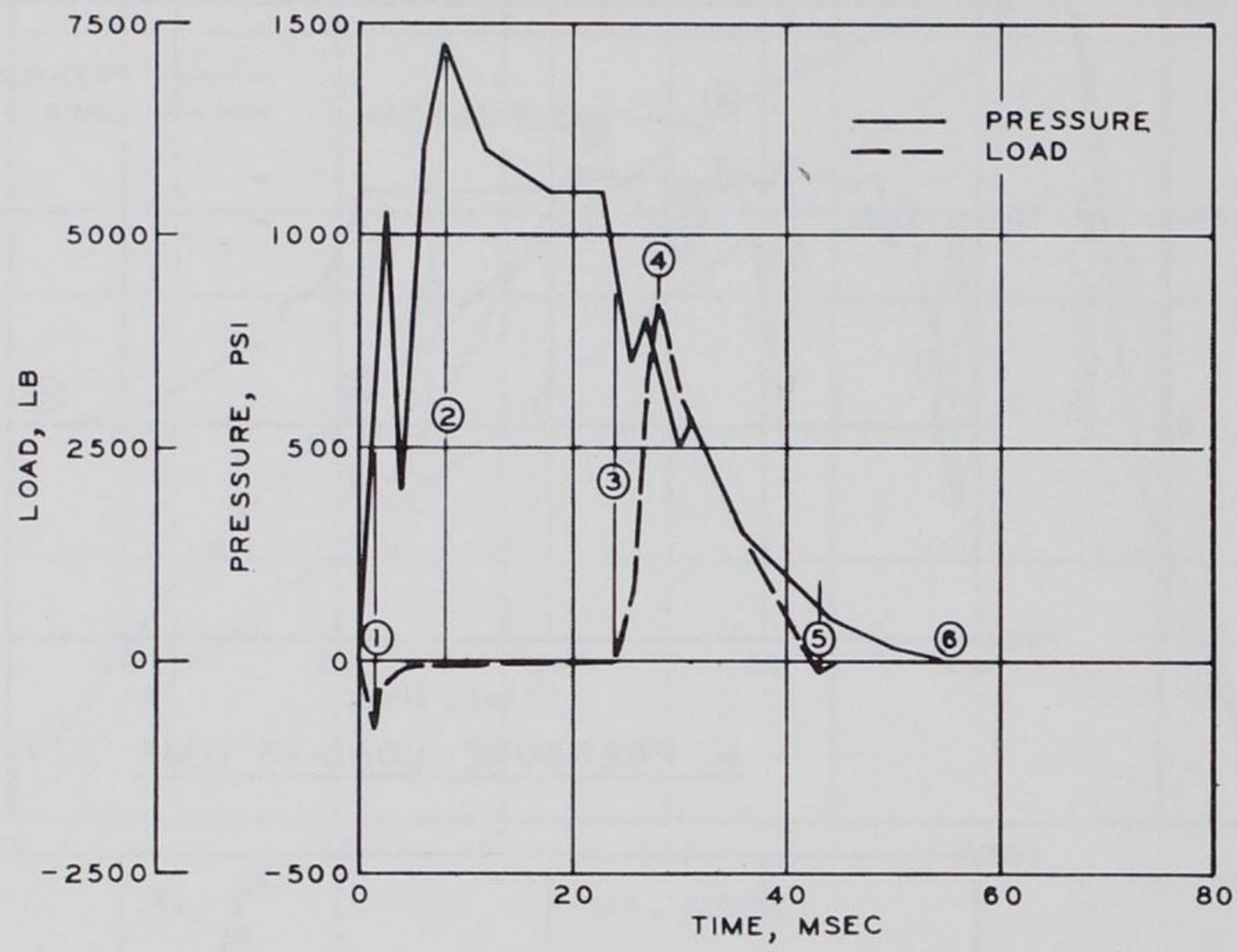

a. PRESSURE-LOAD VS TIME

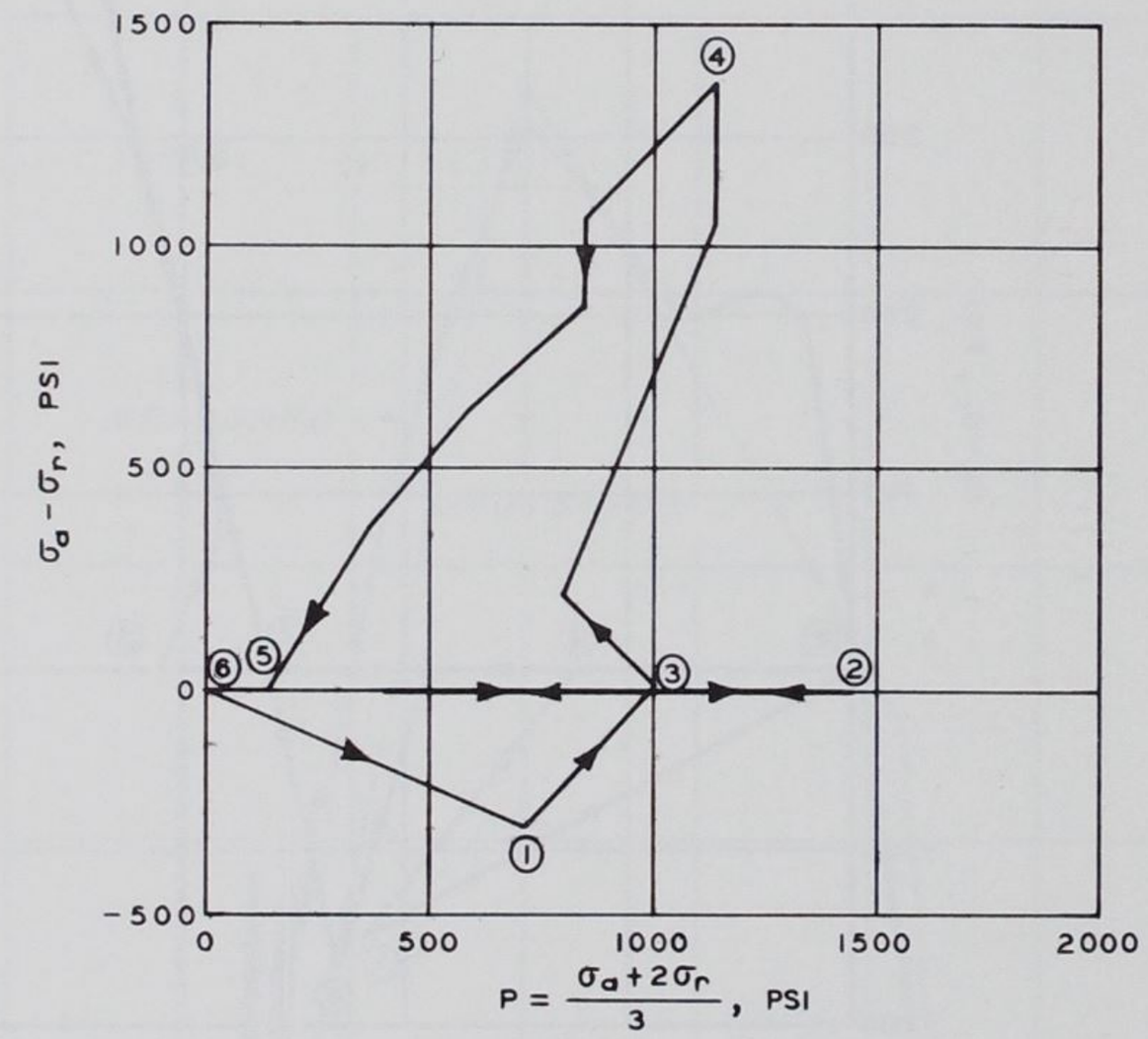

b. STRESS PATH

Figure 4.6 Results of Test 2.2 on clayey silt-stone showing the measured time-history plot of pressure and load and the calculated stress path.

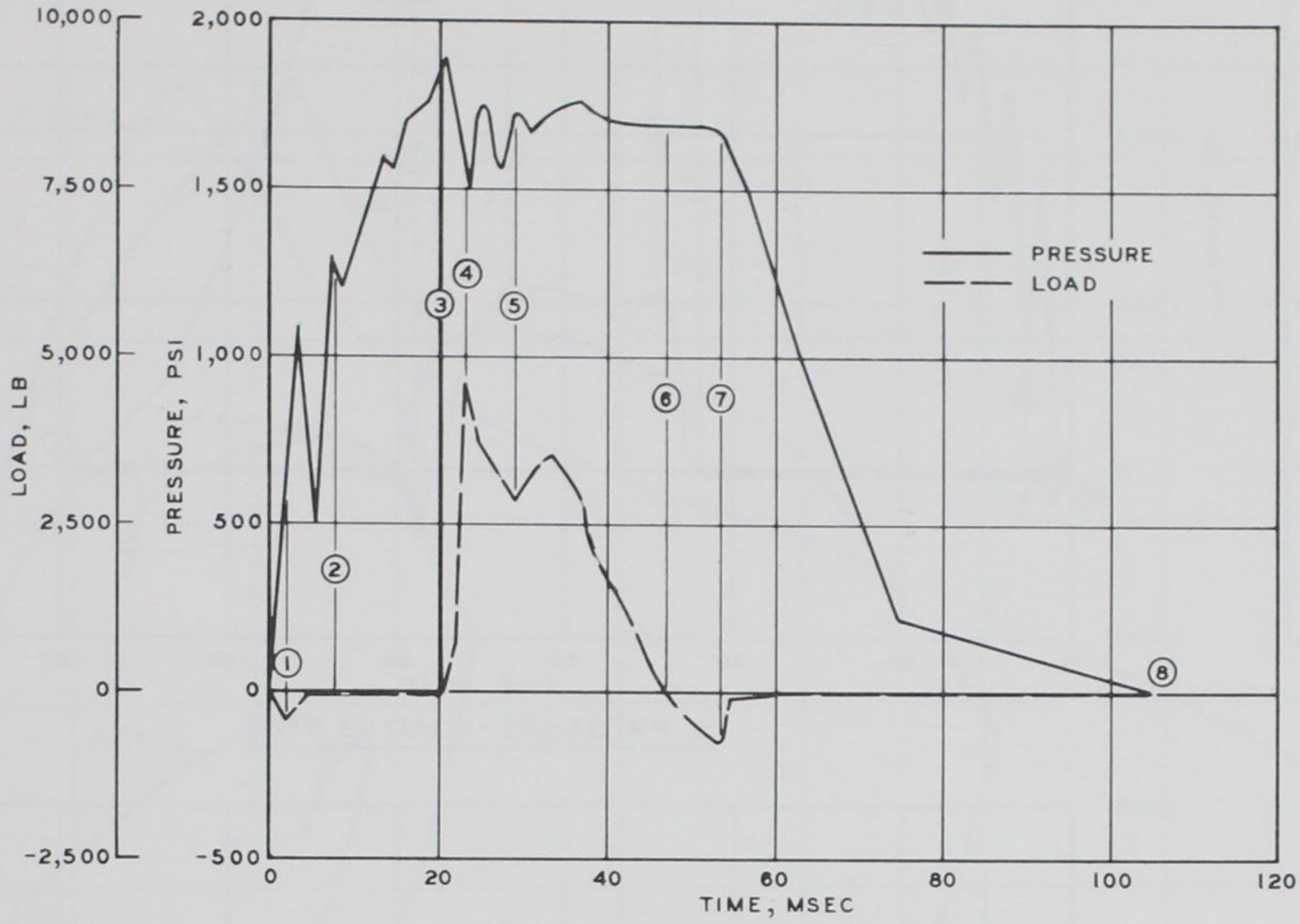

a. PRESSURE-LOAD VS TIME

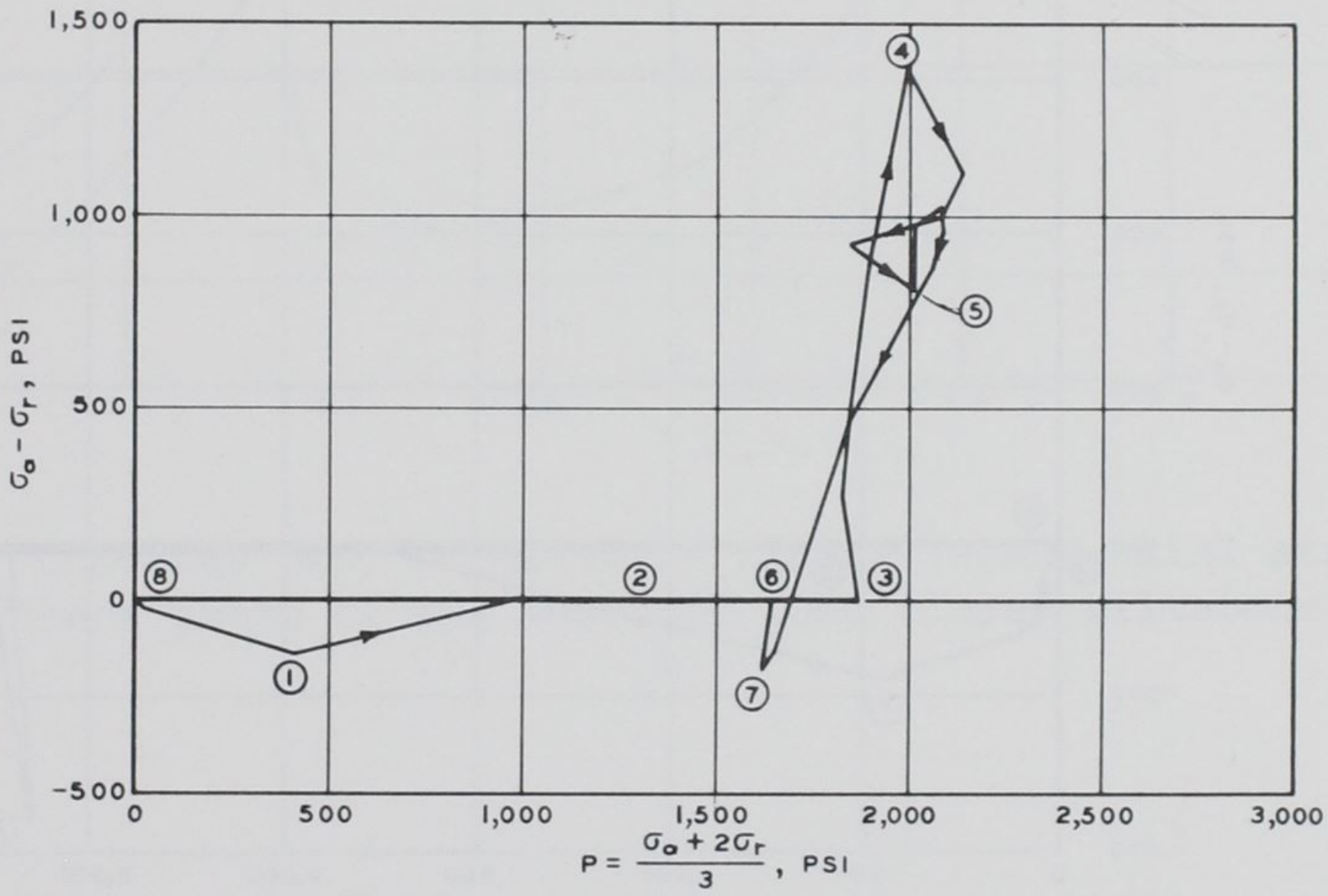

$$P = \frac{\sigma_a + 2\sigma_r}{3}, \text{ PSI}$$

b. STRESS PATH

Figure 4.7 Results of Test 2.3 on clayey siltstone showing the measured time-history plot of pressure and load and the calculated stress path.

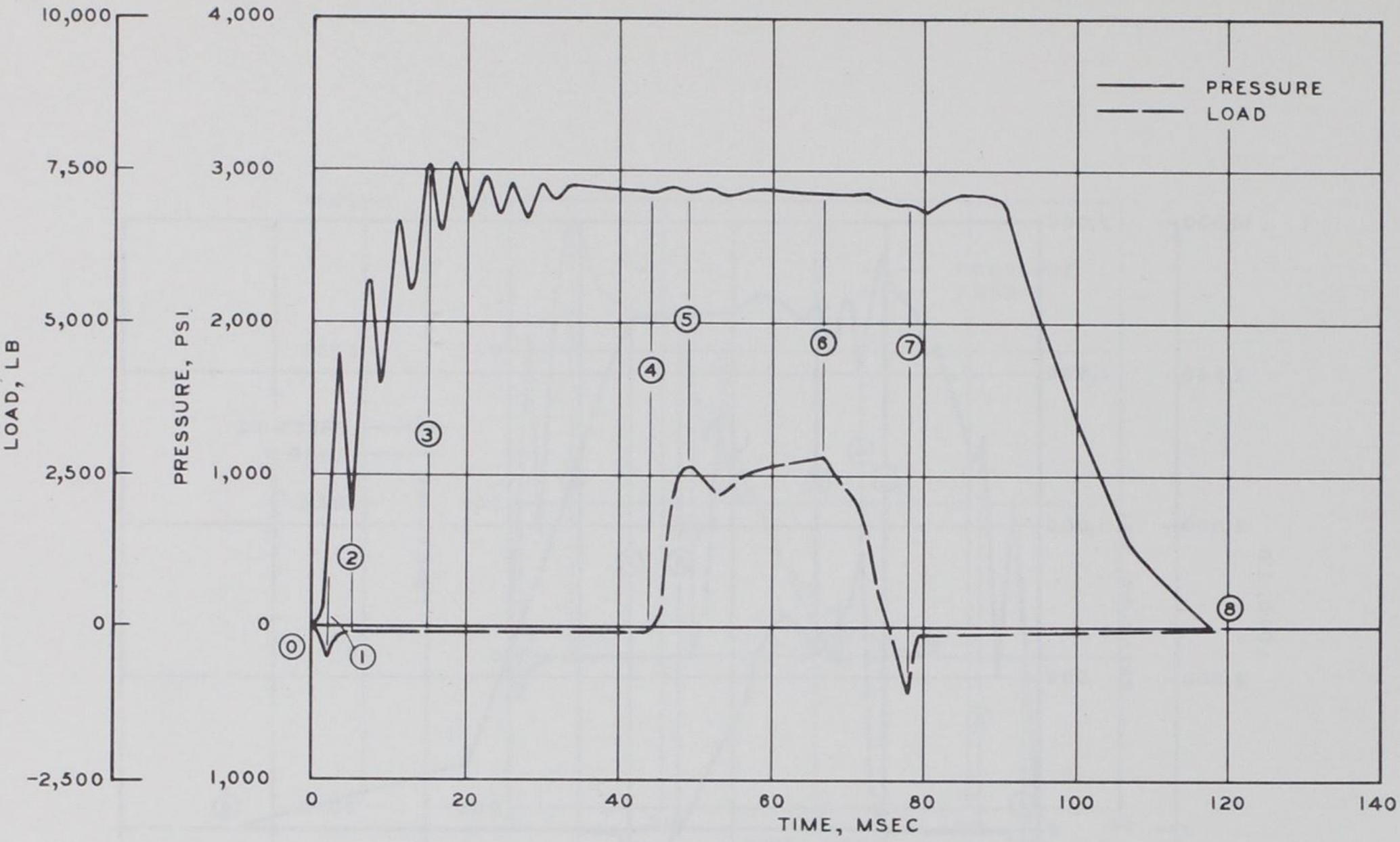

a. PRESSURE - LOAD VS TIME

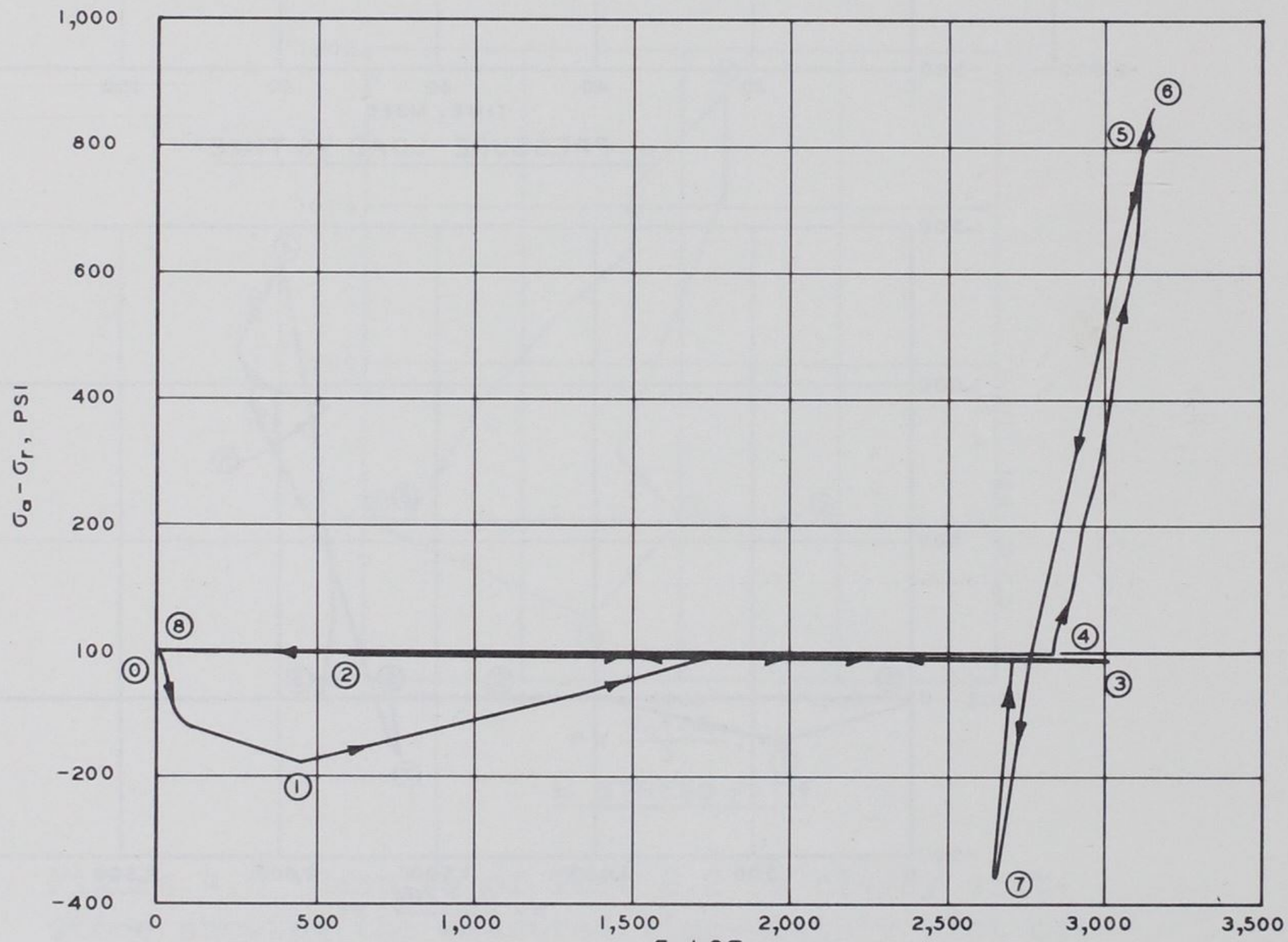

b. STRESS PATH

Figure 4.8 Results of Test 2.4 on clayey siltstone showing the measured time-history plot of pressure and load and the calculated stress path.

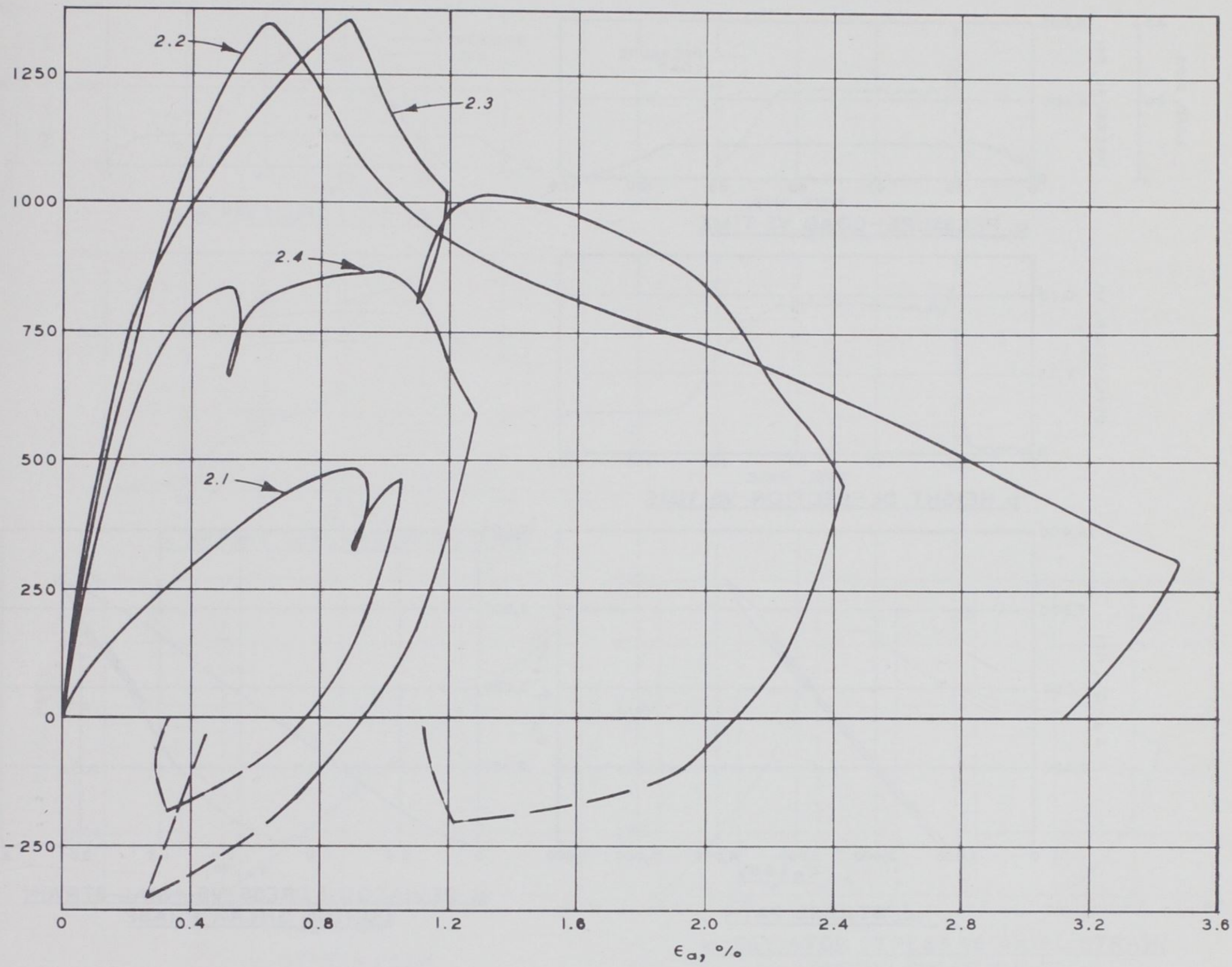

Figure 4.9 Combined plot of deviator stress versus axial strain during the shear phase of the tests of four clayey siltstones.

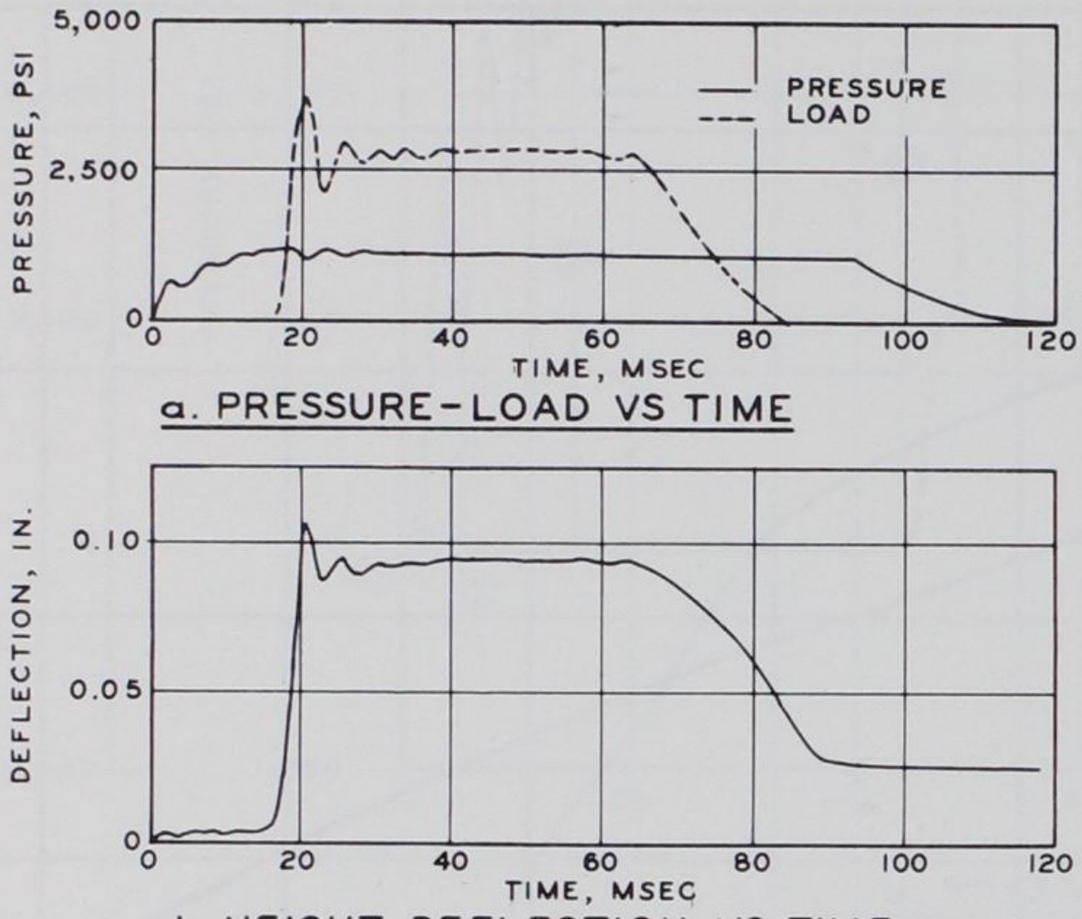

Figure 4.10 Results of Test 3.1 on sandstone showing measured data and calculated stress path and stress-strain plot.

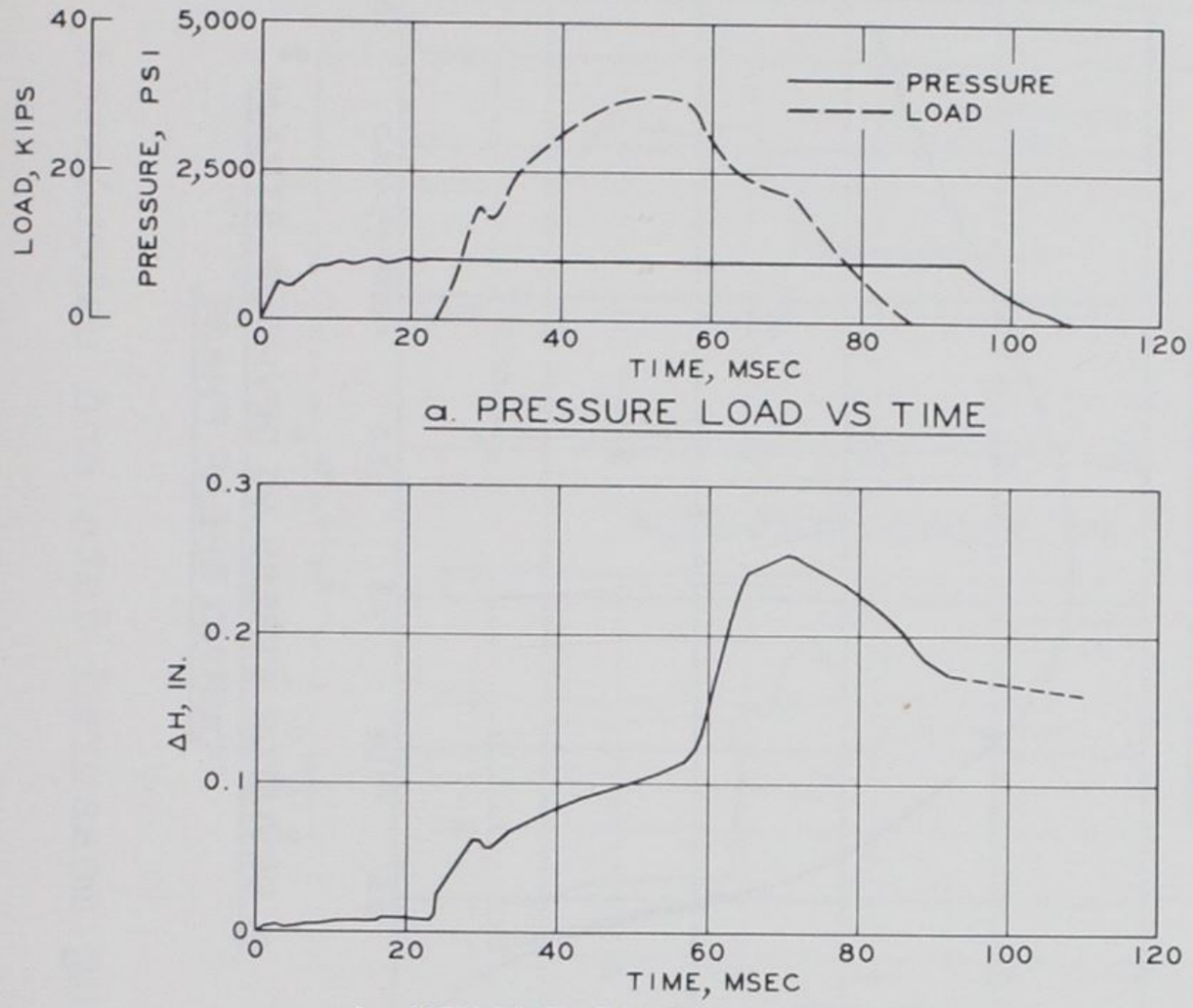

Figure 4.11 Results of Test 3.2 on sandstone showing measured data and calculated stress path and stress-strain plots.

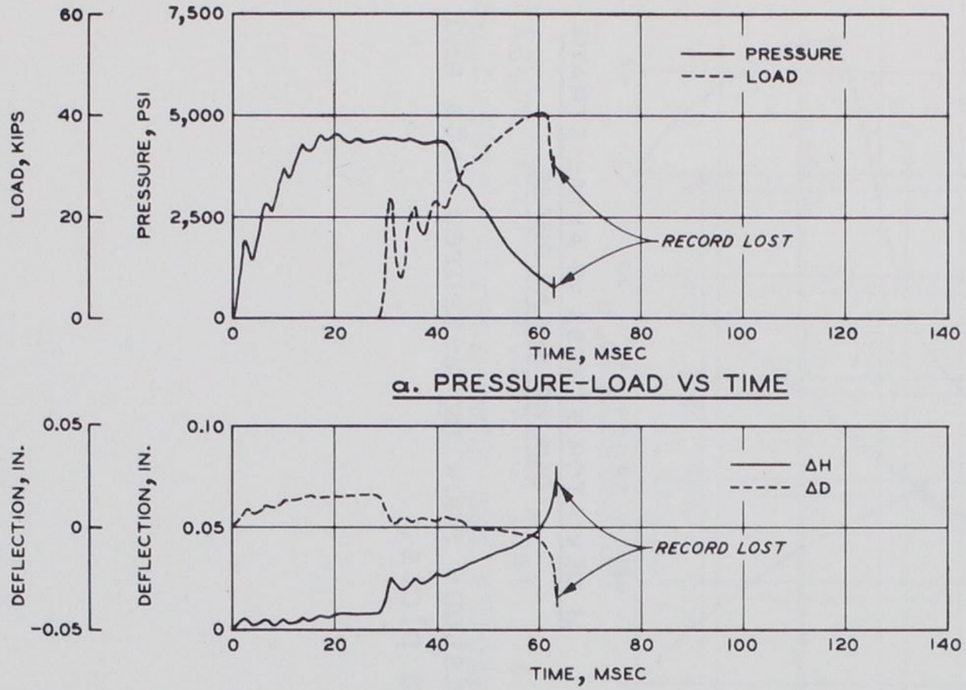

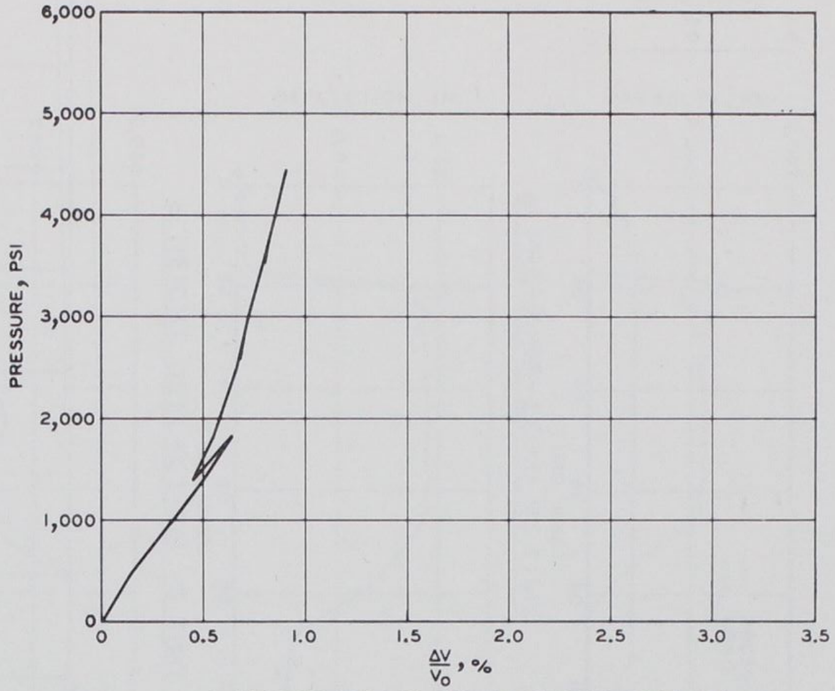

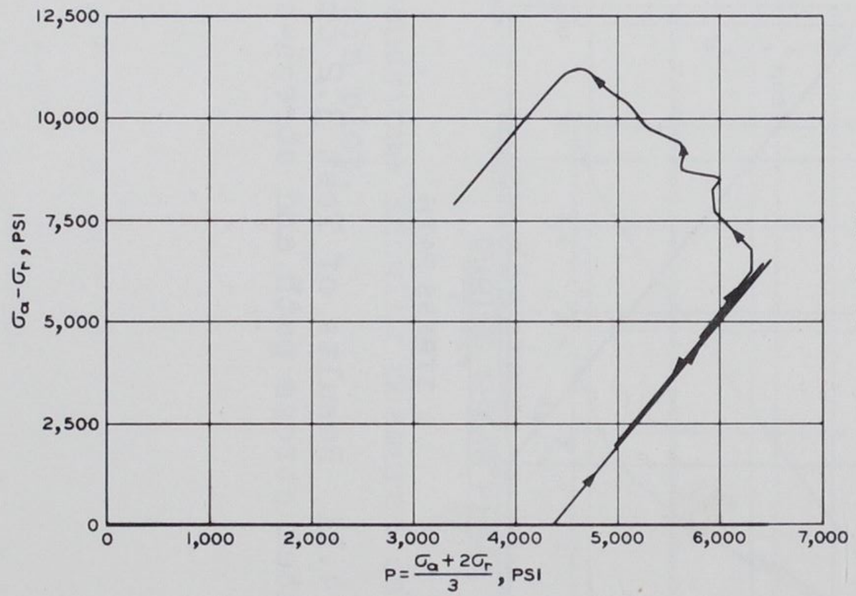

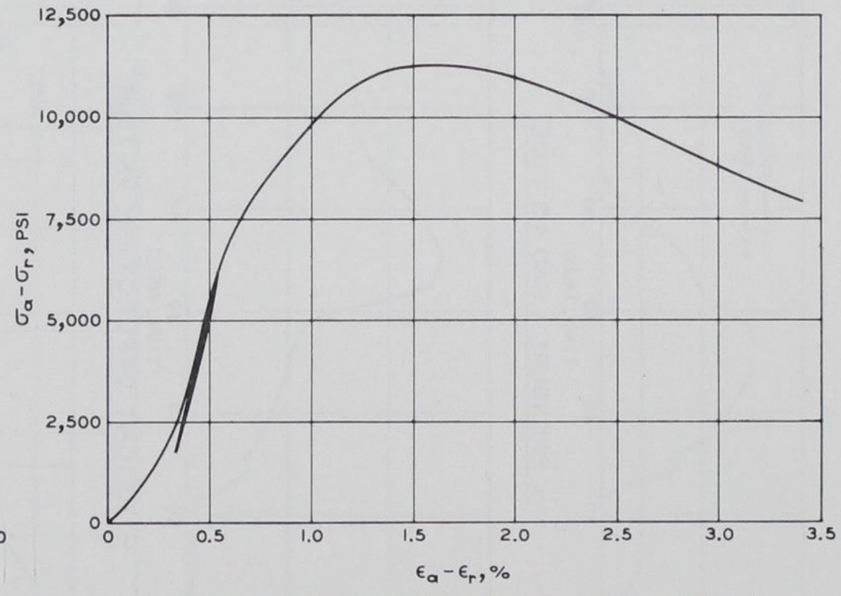

Figure 4.12 Results of Test 3.3 on sandstone showing measured data and calculated stress path and stress-strain plots.

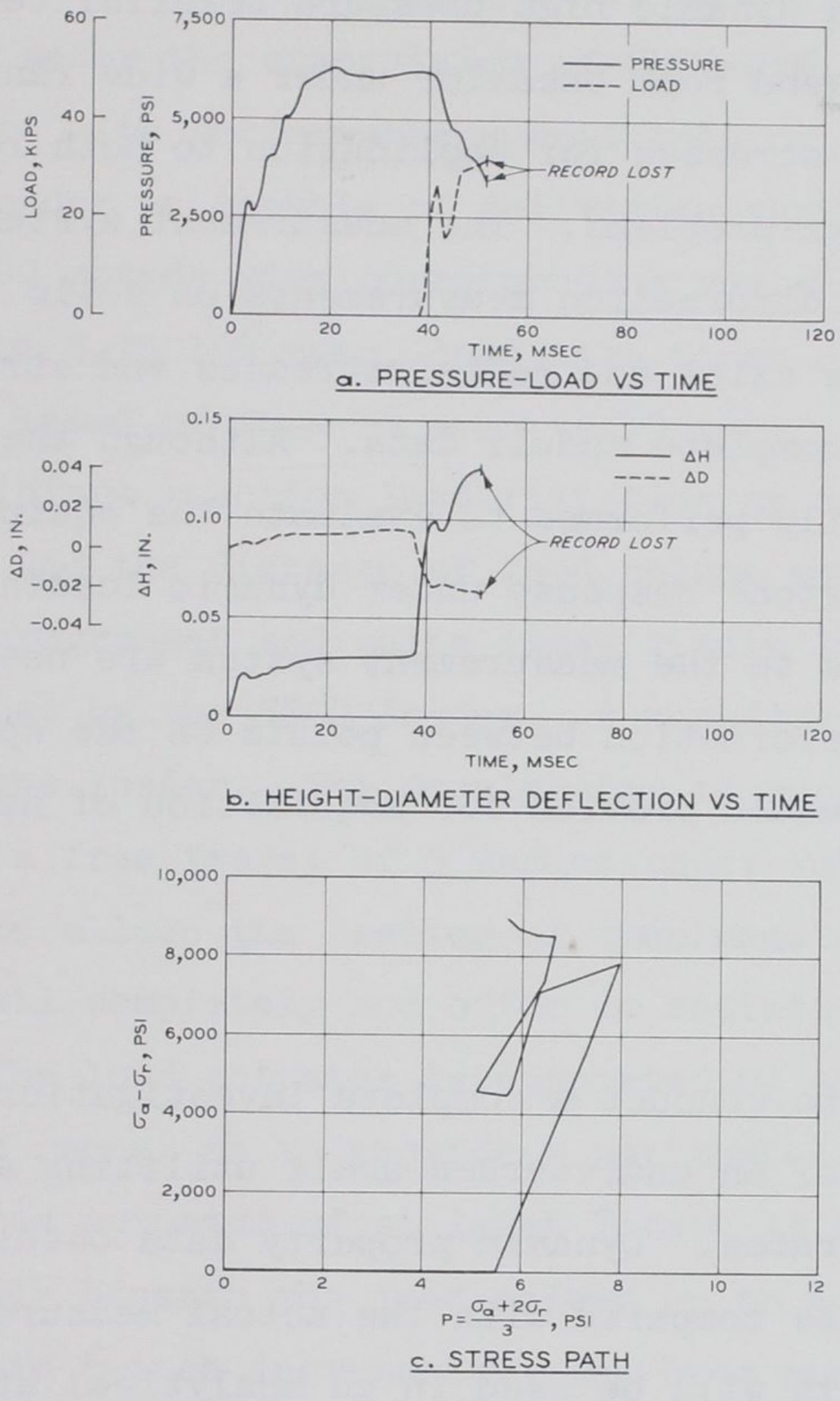

Figure 4.13 Results of Test 3.4 on sandstone showing measured data and calculated stress path and stress-strain plots.

CHAPTER 5

CONCLUSION AND FUTURE PLANS

5.1 CONCLUSION

The successful development of a dynamic high-pressure triaxial testing device allows the study of soil and rock behavior under a wide range of controlled states of impulsive-type stresses for application to both research studies and engineering design problems. The measurement system provides for both axial and lateral deformation measurements on soils and rocks and permits acquisition of the axial and radial stresses and strains necessary for the determination of complete moduli data. Although the tests conducted to date were primarily performed to evaluate the equipment, trends regarding siltstone and sandstone response under dynamic loadings were suggested. Future improvements to the measurement system are needed to allow the measurement of axial deformation between points on the specimen's surface. These improvements would provide for acquisition of negative deviator stress-strain data.

5.2 FUTURE PLANS

Plans are currently under way to conduct a complete investigation into the dynamic stress-strain behavior of an undisturbed shale utilizing a wide range of stress states and loading rates. Dynamic property data obtained by the use of current methods will be compared with the actual measured results. In addition, the test results will be used in an analytical study to investigate boundary condition problems associated with the triaxial device. Studies will also be conducted to provide dynamic yield strength data of a variety of materials. It is hoped that such information will provide insight to material behavior under a variety of states of stress.

APPENDIX A

100-KIP DYNAMIC RAM LOADER

A.1 DESIGN CONSIDERATIONS

The 100-kip ram-type loader (SECO loader) was designed by and fabricated under the supervision of SECO-DYN, Inc., Pomona, California, in compliance with performance specifications and requirements prepared by WES. The loader is capable of delivering variable and controllable loads up to 100,000 pounds with corresponding variable and controllable load rise times of from 3 to 150 msec, load hold times of from 0 to 1,000 msec, and load decay times of from 20 msec to 10 sec. (Specifications actually allowed for minimum reaction load rise time up to 6 msec, depending on the load level and the distance of load column movement.) Loads within 5 percent of that programmed and pulse times within 10 percent of programmed times are obtained by the SECO loader. A nonadjustable decelerator is incorporated into the loader. The decelerator is capable of arresting the load column after a free travel of 5 inches under full load conditions. This safety feature allows the testing of specimens of greater than 5-inch height that may fail completely and offer no resistance to the load column movement.

The load actuator is supported by a stiff beam and support posts in such a manner as to provide a horizontal clear distance directly beneath the load actuator of at least 7 feet 10 inches and clear vertical distances directly beneath the load column up to 4 feet 6 inches above the floor level in 6-inch increments. The beam and posts were designed in such a manner that they would not experience more than 0.03-inch vertical deflection during application of the maximum dynamic load. The overall height of the loader is 11 feet 4 inches so that an existing overhead traveling crane can be used to service the loader and to position it at the desired operating elevation. A photograph of the loader is shown in Figure A.1.

The foundation beneath the loader has been prepared to make it possible to apply loads to a variety of devices and specimens. Two sets of tracks run beneath the loader to accommodate large, rigidly constructed steel test carts in which carefully prepared soil specimens are contained and positioned along the track system for testing. The foundation also

contains a thick, machined plate embedded in the concrete and upon which high-pressure uniaxial strain test devices are positioned for testing. Provisions have also been made for placing a large high-pressure dynamic triaxial test device beneath the loader in order that the loader can be used to apply a synchronized vertical load during a high-pressure dynamic triaxial test.

A.2 OPERATION OF LOADER

The loader is operated with compressed nitrogen, and dynamic load tests are controlled by electrically controlled time valves activated in programmed sequence and by manually controlled orifice valves that are set prior to initiating the load cycle.

A rack of 27 nitrogen bottles is available to supply the loader, with provisions for connecting 18 of the bottles into a common manifold for a supply source. The bottles used are each rated at 2,400 psi. Chambers within the load actuator are pressurized to predetermined levels by valves located in a control console. Pressure in each chamber is monitored by means of gages installed in the control console. A schematic of a section through the actuator is shown in Figure A.2 to illustrate the arrangement and functions of the various chambers.

A.3 DYNAMIC LOAD APPLICATION

To prepare the loader for applying a dynamic load to a specimen or test device, manual adjustment of the load rise and decay control valves is made to produce the rise and decay times desired, and the electrical counters that control the pulse time characteristics by activating the various valves at programmed intervals are set for the desired times. The load actuator is prepared by pressurizing the various chambers (see Figure A.2). First, a 750-psi pressure is applied in the decay-valve-close pressure chamber, and the load column is raised to its uppermost position by application of 25-psi pressure in the column-retract pressure chamber. The rise valve is closed in a similar manner to that used to close the decay valve, and the load generating pressure is introduced into the large force pressure chamber. This pressure varies, of course, with the load to be

delivered. The area of load piston on which the force pressure acts is 56.5 in^2, so the force pressure is approximately equal to the desired load divided by 56.5. Other factors, such as O-ring friction acting on and thus tending to resist movement of the load column, have to be compensated for by adding force pressure. A pressure of 500 psi is introduced into the rise- and decay-valve-open pressure chambers. Normally closed solenoid valves between the valve-close pressure chambers and the valve-lock chambers are then energized, which allows pressurization of the fluid in the valve-lock chambers equal to that in the valve-close pressure chambers, which are simultaneously raised from the original 750 to 1,000 psi. Other normally closed solenoid valves are energized, and the gas in the valve-close pressure chambers is dumped into the atmosphere. The load rise and load decay valves are now held in the closed position by the compressed fluid in the valve-lock chambers. The areas over which the fluid pressures act are such that the opening force resulting from the 500-psi valve-open pressure is overbalanced, and the valves are securely locked in the closed position and the loader in a cocked condition ready for firing. When the test initiate switch is depressed, electrical counters are activated and at programmed intervals activate normally closed solenoid valves. This lets some of the fluid in the rise-valve-lock chamber escape back into an accumulator, thereby reducing the valve locking pressure very rapidly. This allows the 500-psi pressure in the rise-valve-open chamber to push open the rise valve, exposing the port through which the force pressure acts. Complete exposure of the port is accomplished by opening of the valve in less than 1 msec. The rate at which the force pressure acts on the surface of the loading piston is controlled by a series of manually adjusted load-rise-control valves, which were set to produce the desired load-rise times prior to initiating the load cycle. The loader will maintain the load on the load column as long as the pressure is acting on only the upper surface of the load piston. At a preprogrammed interval of time, the counter energizes still another normally closed solenoid valve on the decay system, opening the decay valve in a manner similar to that used in opening the rise valve. Once the load decay valve is open, the force pressure flows through a manually adjusted load decay control valve into the

column-retract pressure chamber and acts on the bottom of the load piston, thereby nullifying the load-generating capacity of the force pressure at a controlled rate.

A.4 STATIC LOAD APPLICATION

The loader can also be used to produce slowly applied loads and to maintain these loads for long periods of time. Prior to this kind of test, the decay valve is closed by 750-psi pressure in the decay-valve-close pressure chamber and the rise valve is forced in the open position to expose the load-rise-control valve parts. By a control valve located in the control console, a predetermined amount of pressure can be admitted into the force pressure chamber at a manually controlled rate. Because the rise valve has been placed in an open position, the pressure acts directly on the load piston, thus generating the desired load. Loads applied in this manner can be maintained indefinitely. Removal of the load is accomplished by simply exhausting the force pressure.

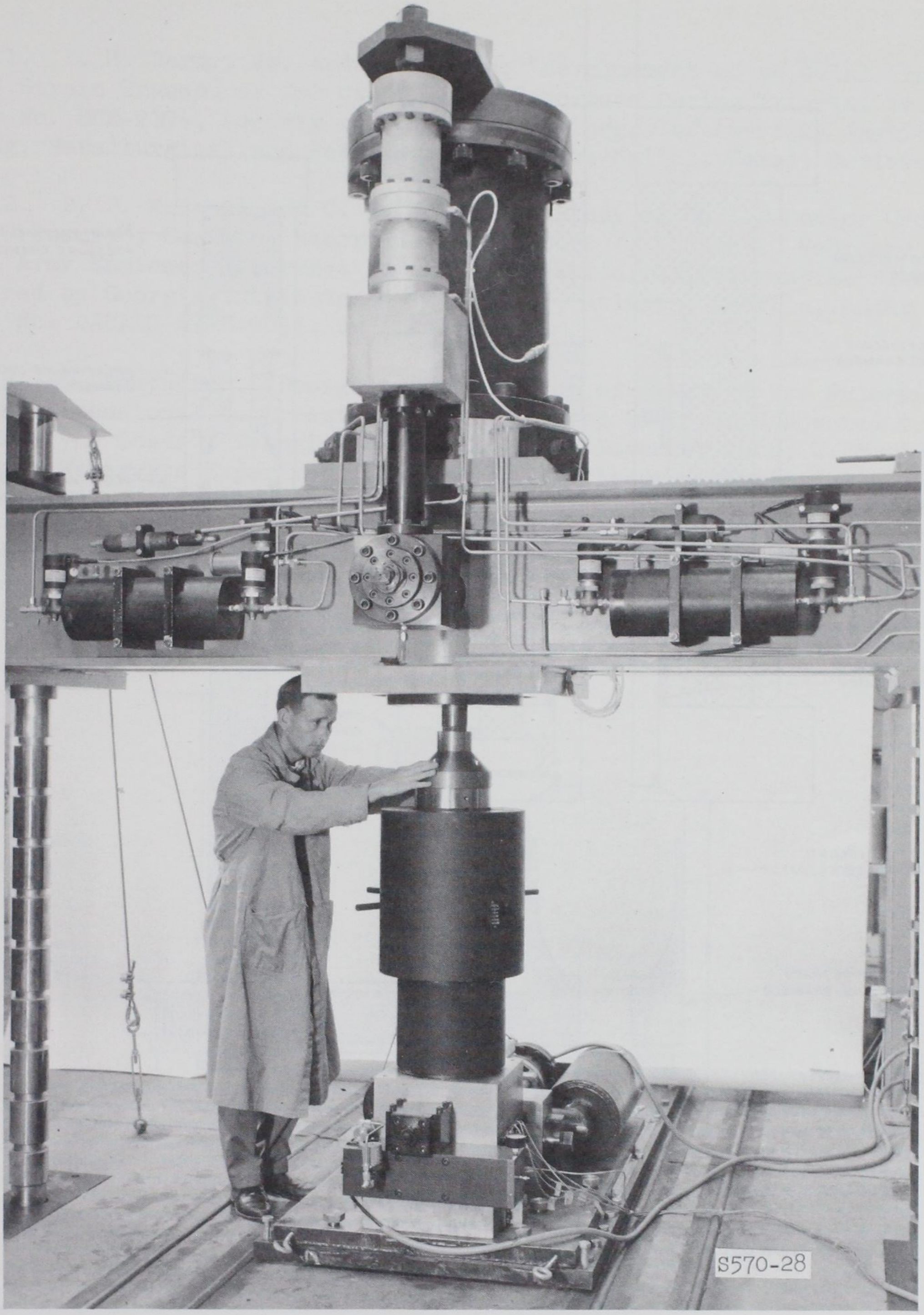

Figure A.1 The 100-kip dynamic ram loader with the dynamic high-pressure triaxial device in the assembled test position.

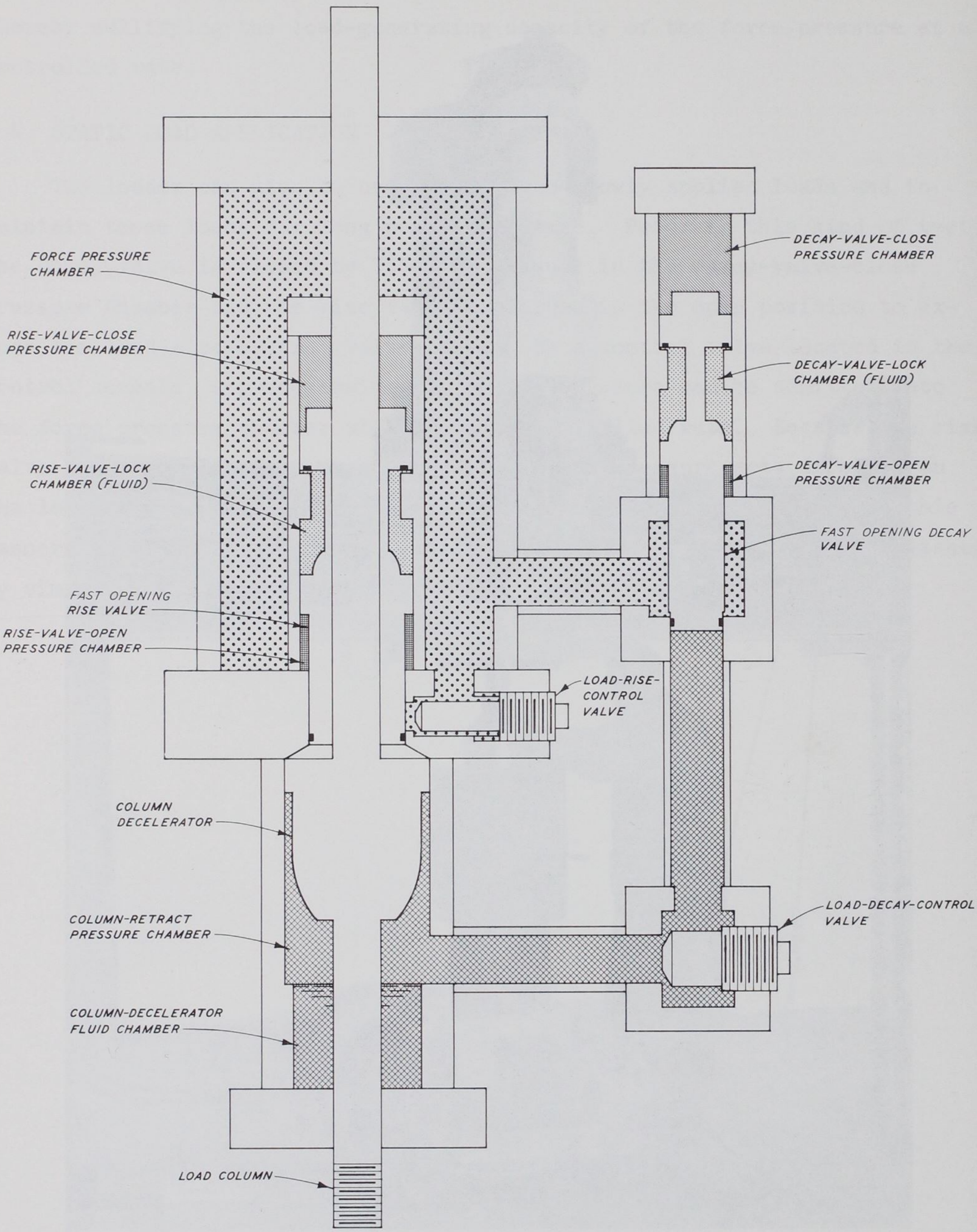

Figure A.2 Actuator of the 100-kip dynamic loader.

REFERENCES

1. H. R. Hardy, Jr. and Y. S. Kim; "Development of an Axial Transverse Strain Transducer for Use on Rock Specimens During Triaxial Tests"; Paper No. SPE-2394, Society of Petroleum Engineers of American Institute of Mining, Metallurgical and Petroleum Engineers, Dallas, Texas; Unclassified.

2. B. B. Mazanti and C. N. Holland; "Study of Soil Behavior Under High Pressure"; Contract Report S-70-2, Report 1, Volume 1, February 1970; U. S. Army Engineer Waterways Experiment Station, CE, Vicksburg, Mississippi, prepared by Georgia Institute of Technology, Atlanta, Georgia, under Contract No. DACA39-67-C-0051; Unclassified.

3. L. Schindler; "Design and Evaluation of a Device for Determining the One-Dimensional Compression Characteristics of Soils Subjected to Impulse-Type Loads"; Technical Report S-68-9, November 1968; U. S. Army Engineer Waterways Experiment Station, CE, Vicksburg, Mississippi; Unclassified.

4. W. R. Wozwersik; "Detailed Analysis of Rock Failure in Laboratory Compression Tests"; Ph. D. dissertation, July 1968; University of Minnesota, Minneapolis, Minnesota; Unclassified.

DISTRIBUTION LIST FOR TECHNICAL REPORT S-71-15

Address	No. of Copies

Army

Chief of Engineers, Department of the Army, Washington, D. C. 20314
ATTN: ENGMC-ED 1
ENGAS-I 1

Division Engineer, U. S. Army Engineer Division, Huntsville,
P. O. Box 1600, West Station, Huntsville, Ala. 35807
ATTN: Mr. T. R. Wathen 1
Mr. M. M. Dembo 1

Director of Civil Defense, Office of the Secretary of the Army, 1
Washington, D. C. 20310
ATTN: Engineering Development Division (Research Directorate)

Chief of Research and Development, Department of the Army,
Washington, D. C. 20310
ATTN: CRDNCB 1
CRDES 1

Chief of Research and Development, Department of the Army, 3 copies
Washington, D. C. 20310 of Form
ATTN: Director of Army Technical Information 1473

Director, Explosive Excavation Research Office, U. S. Army 1
Engineer Waterways Experiment Station, P. O. Box 808,
Livermore, Calif. 94550

Commanding Officer, U. S. Army Nuclear Defense Laboratory, 1
Edgewood Arsenal, Edgewood, Md. 21040
ATTN: Technical Library

Director, U. S. Army Cold Regions Research and Engineering 1
Laboratory, P. O. Box 282, Hanover, N. H. 03755
ATTN: Mr. K. Boyd

Commanding Officer, Army Materials and Mechanics Research 1
Center, Watertown, Mass. 02172
ATTN: Dr. Arfon Jones

Address	No. of Copies
Navy	
Commander, Naval Facilities Engineering Command, Navy Department, Washington D. C. 20370	
ATTN: Code 04	1
Code 03	1
Chief of Naval Research, Navy Department, Washington, D. C. 20390	1
ATTN: Code 811	
Commanding Officer & Director, U. S. Naval Civil Engineering Laboratory, Port Hueneme, Calif. 93041	
ATTN: Library	1
Mr. C. R. White	1
Mr. H. L. Gill	1
Air Force	
Air Force Weapons Laboratory, Kirtland AFB, N. Mex. 87117	
ATTN: Library	1
WLDC	1
Dr. H. F. Cooper, Jr.	1
CPT H. E. Selheimer	1
Space and Missile Systems Organization, Norton AFB, Calif. 92409	
ATTN: SMQHE	1
SMQHF-1	1
Director of Civil Engineering, Headquarters, USAF, Washington, D. C. 20330	1
ATTN: AFOCE	
Director, U. S. Air Force Project RAND, Via: U. S. Air Force Liaison Office, The Rand Corporation, 1700 Main Street Santa Monica, Calif. 90406	1
ATTN: Library	
Colleges and Universities	
University of California, Lawrence Radiation Laboratory, P. O. Box 808, Livermore, Calif. 94550	
ATTN: Technical Information Division	1
Dr. F. J. Tokarz, L-90	1

Address	No. of Copies

Colleges and Universities (Continued)

The Citadel, COL Himelright, Civil Engineering Department, Charleston, S. C. 29409	1
City College of New York, Department of Civil Engineering, New York, N. Y. 10010 ATTN: Dr. O. J. Costantino	1
Columbia University, Professor Robert D. Stoll, 638 Seeley W. Mudd Building, New York, N. Y. 10027	1
Duke University, Department of Civil Engineering, Durham, N. C. 27706 ATTN: Professor Aleksander B. Vesic	1
University of Florida, Civil Engineering Department, Gainesville, Fla. 32601 ATTN: Professor J. H. Schmertmann	1
Georgia Institute of Technology, School of Civil Engineering, Atlanta, Ga. 30332 ATTN: Dr. B. B. Mazanti	1
Howard University, Department of Civil Engineering, Washington, D. C. 20001 ATTN: Dr. Delon Hampton	1
University of Illinois, Department of Civil Engineering, Urbana Campus, Urbana, Ill. 61801	
ATTN: Professor A. J. Hendron, Jr.	1
Professor N. M. Newmark	1
Professor R. B. Peck	1
University of Kentucky, Department of Civil Engineering, Lexington, Ky. 40506 ATTN: Professor B. O. Hardin	1
Louisiana State University, Department of Civil Engineering, Baton Rouge, La. 70803 ATTN: Dr. J. K. Poplin	1
The University of Michigan, Department of Civil Engineering, Ann Arbor, Mich. 48104 ATTN: Professor F. E. Richart, Jr.	1

Address	No. of Copies

Colleges and Universities (Continued)

University of New Mexico, Civil Engineering Research Facility, P. O. Box 188, University Station, Albuquerque, N. Mex. 87106	
ATTN: Mr. Delmar E. Calhoun	1
Dr. G. Triandafilidis	1
State University of New York, Department of Civil Engineering, Buffalo, N. Y. 14214	1
ATTN: Dr. Ernest T. Selig	
North Carolina State University, Box 5628, Raleigh, N. C. 27607	1
ATTN: Professor Ralph E. Fadum	
Northwestern University, Department of Civil Engineering, Technological Institute, Evanston, Ill. 60201	1
ATTN: Associate Professor Raymond J. Krizek	
Purdue University, School of Civil Engineering, Lafayette, Ind. 47907	1
ATTN: Professor Gerald A. Leonards	
University of Texas, Civil Engineering Department, Austin, Tex. 78712	1
ATTN: Professor H. Neils Thompson	
University of Utah, Department of Mechanical Engineering, Salt Lake City, Utah 84112	1
ATTN: Dr. Wayne Brown	
Massachusetts Institute of Technology, Division of Sponsored Research, 77 Massachusetts Avenue, Cambridge, Mass. 02139	1
ATTN: Dr. Robert V. Whitman	
California Institute of Technology, Division of Engineering, Pasadena, Calif. 91109	1
ATTN: Dr. Ronald Scott	
University of California, Room 301, Engineering Materials Laboratory, Berkeley, Calif. 94720	1
ATTN: Professor H. Bolton Seed	
Texas A&M University, Department of Civil Engineering, College Station, Tex. 77843	
ATTN: Professor L. J. Thompson	1
Professor W. A. Dunlap	1
Professor J. Handin	1

Address	No. of Copies

Colleges and Universities (Continued)

Brown University, Division of Engineering, Providence, R. I. 02912 ATTN: Dr. W. Prager	1
George Washington University, Department of Engineering Mechanics, Washington, D. C. 20006 ATTN: Dr. A. Freudenthal	1

Other

Professor Arthur Casagrande, 16 Rockmont Road, Belmont, Mass. 02178	1
E. D'Appolonia Consulting Engineers, Inc., 10 Duff Road, Pittsburgh, Pa. 15235 ATTN: Dr. John R. Hall, Jr.	1
Director, Advanced Research Projects Agency, The Pentagon, Washington, D. C. 20315 ATTN: Dr. Stanley Ruby (NMRO-RM. 3D170)	1
Aerospace Corporation, 1111 E. Mill Street, San Bernardino, Calif. 92408	
ATTN: Dr. S. B. Batdorf	1
Dr. M. B. Watson	1
Agbabian-Jacobsen Associates, Engineering Consultants, 8939 South Sepulveda Boulevard, Los Angeles, Calif. 90045	1
Applied Theory Incorporated, 1010 Westwood Boulevard, Los Angeles, Calif. 90024	
ATTN: Dr. John G. Trulio	1
Battelle Memorial Institute, 505 King Avenue, Columbus, Ohio 43201	
ATTN: Mr. R. W. Klingesmith	1
Dr. P. N. Lamari	1
The Boeing Company, Aerospace Group, Missile and Information Systems Division, P. O. Box 3985, Seattle Wash. 98124	
ATTN: Mr. H. G. Leistner	1
Mr. Joel K. Bloomer	1
Director, Defense Nuclear Agency, Washington, D. C. 20301 ATTN: SPSS	5

Address	No. of Copies

Other (Continued)

Defense Documentation Center (DDC), Cameron Station, 12
Alexandria, Va. 22314
ATTN: Mr. Myer Kahn
(NO TOP SECRET TO THIS ADDRESS)

Director of Defense Research and Engineering, 1
Washington, D. C. 20301
ATTN: Technical Library

Defence Research Establishment, Suffield, Ralston, 1
Alberta, Canada

Denver Mining Research Center, Building 20, Denver Federal Center, 1
Denver, Colo. 80225
ATTN: Dr. Leonard A. Obert

General Electric Company, TEMPO, 816 State Street, 1
Santa Barbara, Calif. 93101
ATTN: Mr. Warren Chan (DASIAC)

General Motors Corporation, Manufacturing Development, 1
Technical Center, Warren, Mich. 48090
ATTN: Mr. W. M. Isbell

IIT Research Institute, 10 West 35th Street, Chicago, Ill. 60616
ATTN: Library 1
Dr. E. Vey 1

Sandia Laboratories, P. O. Box 5800, Kirtland AFB, N. Mex. 87115
ATTN: Classified Document Division for Dr. M. L. Merritt 1
Mr. C. W. Gulick, Division 9133 1
Mr. W. R. Perret 1
Dr. W. Von Riesemann, Division 1541 1

Systems, Science & Software, P. O. Box 1620, 1
La Jolla, Calif. 92037
ATTN: Mr. Robert T. Allen

Commander, Test Command, Defense Nuclear Agency, 1
Kirtland Air Force Base, N. Mex. 87115
ATTN: TCCOM, TCDT

Address	No. of Copies
Other (Continued)	
Physics International Company, 2700 Merced Street, San Leandro, Calif. 94577	
ATTN: Dr. Charles Godfrey	1
Mr. Fred M. Sauer	1
TRW Systems, One Space Park, Redondo Beach, Calif. 90278	
ATTN: Dr. Peter Dai	1
Mr. Norman Lipner	1
TRW Systems, P. O. Box 1310, San Bernardino, Calif. 92402	1
ATTN: Mr. Fred A. Pieper	
Paul Weidlinger, Consulting Engineer, 110 East 59th Street, New York, N. Y. 10022	
ATTN: Dr. M. L. Baron	1
Dr. Ivan Nelson	1
Mr. G. F. Weissmann, Room 1B-124, Bell Telephone Laboratories, Murray Hill, N. J. 07971	1
Shannon and Wilson, Incorporated, 1105 North 38th Street, Seattle, Wash. 98103	1
ATTN: Mr. Earl A. Sibley	

Unclassified
Security Classification

DOCUMENT CONTROL DATA - R & D

(Security classification of title, body of abstract and indexing annotation must be entered when the overall report is classified)

1. ORIGINATING ACTIVITY *(Corporate author)*

U. S. Army Engineer Waterways Experiment Station
Vicksburg, Mississippi

2a. REPORT SECURITY CLASSIFICATION

Unclassified

2b. GROUP

3. REPORT TITLE

DEVELOPMENT OF A DYNAMIC HIGH-PRESSURE TRIAXIAL TEST DEVICE

4. DESCRIPTIVE NOTES *(Type of report and inclusive dates)*

Final report

5. AUTHOR(S) *(First name, middle initial, last name)*

John Q. Ehrgott
Richard C. Sloan

6. REPORT DATE

November 1971

7a. TOTAL NO. OF PAGES

75

7b. NO. OF REFS

4

8a. CONTRACT OR GRANT NO.

b. PROJECT NO. DNA Subtask SB209A

c.

d.

9a. ORIGINATOR'S REPORT NUMBER(S)

Technical Report S-71-15

9b. OTHER REPORT NO(S) *(Any other numbers that may be assigned this report)*

10. DISTRIBUTION STATEMENT

Approved for public release; distribution unlimited.

11. SUPPLEMENTARY NOTES

12. SPONSORING MILITARY ACTIVITY

Defense Nuclear Agency
Washington, D. C.

13. ABSTRACT

A unique dynamic high-pressure triaxial test device has recently been developed at the U. S. Army Engineer Waterways Experiment Station to assist in obtaining dynamic stress-strain and strength data for use in formulating soil and rock constitutive relations used in blast-induced ground shock calculations. The device is capable of imposing controlled impulsive-type confining pressures up to 15 kips/in^2 on specimens up to 3 inches in diameter; peak pressures can be achieved in as little time as 3 msec, and all pressure can be removed in 20 msec. These dynamic confining pressures can be time-synchronized with similar dynamic axial load pulses with magnitudes up to 100 kips. Independent control of the axial and radial stresses permits application of dynamic hydrostatic loadings and unloadings to obtain bulk moduli; dynamic deviatoric loadings under constant confining pressure to obtain Young's moduli and yield stress data; dynamic deviatoric loadings while maintaining a condition of constant mean normal stress to obtain shear moduli; and a variety of other loadings including constant stress ratios. This report presents a description of the dynamic, high-pressure triaxial device, which consists basically of five components, i.e., the rise pressure supply system, the decay system, the base assembly, the triaxial chamber, and the stroke limiter. Details of the measurement systems used for determination of confining pressure, axial load, and axial and lateral deformation under dynamic high-pressure fluid environments are given. Several results from an evaluation test series conducted on field NX-size cores of a clayey siltstone and Cretaceous sandstone are presented to demonstrate some of the capabilities of the device and to show the type of dynamic stress paths the device is capable of generating. The data are shown as time-history plots of confining pressure and axial load for the complete hydrostatic and shear phases of the tests along with the corresponding stress path plots of deviator stress versus mean normal stress. Deviator stress versus axial strain plots are also shown for the shear phase. The results illustrate that the device is not only useful in site investigations in which determination of dynamic properties of the material encountered is required for engineering design purposes, but also in fundamental research studies to determine material behavior under a variety of states of impulsive-type stresses.

DD FORM 1 NOV 68 1473 REPLACES DD FORM 1473, 1 JAN 64, WHICH IS OBSOLETE FOR ARMY USE.

Unclassified
Security Classification

14. KEY WORDS	LINK A		LINK B		LINK C	
	ROLE	WT	ROLE	WT	ROLE	WT
Dynamic pressure						
Ground shock						
Rock properties						
Rock test specimens						
Test equipment						
Triaxial tests						